A Numerical Study of the Effect of Island Terrain on Tropical Cyclones

MORRIS A. BENDER, ROBERT E. TULEYA AND YOSHIO KURIHARA

Geophysical Fluid Dynamics Laboratory/NOAA, Princeton University, Princeton, NJ 08542

(Manuscript received 20 March 1986, in final form 2 July 1986)

ABSTRACT

A triply nested, movable mesh model was used to study the behavior of tropical cyclones encountering island mountain ranges. The integration domain consisted of a 37° wide and 45° long channel, with an innermost mesh resolution of ⅙°. The storms used for this study were embedded in easterly flows of ~5 and ~10 m s^{-1} initially. Realistic distributions of island topography at ⅙° resolution were inserted into the model domain for the region of the Caribbean, including the islands of Cuba, Hispaniola, and Puerto Rico; the island of Taiwan; and the region of Luzon in the northern Philippines.

It was found that the islands affected the basic flow as well as the wind field directly associated with the storm system. The combination of these effects caused changes in the track and translational speed of the storm. In particular, in the case of the 5 m s^{-1} easterly flow, the storm accelerated and veered to the north well before reaching Taiwan. For the other island distributions, the northward deflection of the track and the increase of translational speed occurred near and over the islands. After landfall, the surface pressure underwent rapid filling. As the tropical cyclone passed over Hispaniola, the surface low continued to move along with the upper level vortex as it transversed the mountain range, while over Luzon it became obscure before reforming on the lee side slope of the mountain. In case of Taiwan and the 10 m s^{-1} easterly zonal flow, secondary surface lows developed behind the mountain range. The upper level vortex in this case became detached from the original surface low and eventually coupled with a secondary one.

The intensity changes of the storm near and over the islands were strongly related to the latent energy supply and the vertical coherence of the storm system. Advection of dry air from near or above the mountain tops into the storm area caused significant weakening of all the storms moving with the weaker easterly flow. Storms leaving Hispaniola and moving over open sea quickly reintensified as their vertical structure remained coherent. On the other hand, storms leaving Luzon were disorganized and did not reintensify until several hours later when the vertical coherence of the systems was reestablished.

Although these experiments were performed for an idealized experimental design and basic flow, many observed storms have exhibited similar behavior in track deviation and decay. This implies that the effect of detailed topography should be considered if an accurate forecast of the storm direction and behavior is to be made.

1. Introduction

The behavior of tropical cyclones is often affected by many factors including the various environmental conditions surrounding them. Although the interaction with the terrain is one factor of great interest and practical importance, many of the details of this interaction are not well understood. Yet, in many places with large tropical cyclone threats the terrain of the region is quite mountainous.

Still, apparent influences of orography on the movement of tropical cyclones have been observed. For example, increases in the storm's translational speed have been reported in statistical studies by Brand and Blelloch (1973) and observations by Kintanar et al. (1974) for typhoons approaching and transversing the mountainous terrain of the northern Philippines. Northward perturbations of the track for these storms have also been noted by Brand and Blelloch (1973). A distinct northward deflection in the tracks of storms approaching the island of Taiwan has also been observed by Brand and Blelloch (1974) who observed a typical southward deflection as the storms leave the island. These results have been shown for many individual cases by Wang (1980) who has summarized the path and behavior of 53 typhoons approaching Taiwan. Also, interaction with the high mountains of Hispaniola may have contributed to the sharp northward deflection in the paths of Hurricane David and Tropical Storm Frederic as they approached south of the island (Hebert, 1980).

These authors have also noted rapid decay of the storm systems as they interacted with the mountainous topography of the regions. For example, Brand and Blelloch (1974) noted that the value of the maximum surface winds typically decreased over 40%, beginning about 12 h before the tropical cyclone centers reach the island of Taiwan. Hurricane David also rapidly decayed to tropical storm strength as it crossed Hispaniola (Hebert, 1980), filling 76 mb in 18 h.

Another important quantity often affected by the presence of mountainous terrain is the storm rainfall

distribution. Observations by many authors (e.g., Brunt, 1968; Hamuro et al., 1969) have confirmed the high correlations that exist between areas of maximum rainfall during the landfall of tropical cyclones and the mountainous terrain of the region.

In most of the examples given so far, the significant orographic effects on the behavior of tropical cyclones have apparently been caused by island mountain ranges. Indeed, many of the regions in the world with the greatest tropical cyclone threat such as Taiwan, Japan, or Madagascar, are island areas which contain significant mountainous terrain. Some of these important orographic influences were first numerically simulated by Chang (1982) in a primitive equation model which included a simplified island mountain range similar to that of Taiwan. Some of the mountain interactions with a typhoon-like vortex have also been reproduced in laboratory models for the island of Taiwan (e.g., Pao and Hwang, 1977), and for a region of the Philippine islands (e.g., Brand et al., 1982).

Idealized numerical simulations of the landfall of tropical cyclones have been performed previously by Tuleya and Kurihara (1978); Moss and Jones (1978); and Tuleya, Bender, and Kurihara (1984) without the effect of orography included. More recently, this effect was studied by Bender, Tuleya, and Kurihara (1985; hereafter referred to as BTK) in a numerical landfall simulation in which an idealized mountain range was placed parallel to the shoreline. Many effects that such a mountain range may produce on landfalling tropical cyclones were investigated in this study. However, it remained uncertain how much these effects could be generalized with the introduction of more realistic topographical distributions. The present study, which is a continuation of this earlier work, attempts to address this question. In particular, three different island distributions at very fine resolution ($\frac{1}{6}°$) were chosen and placed into the model domain. Since the magnitude of the basic flow is often an important parameter to be considered whenever the mountain effects on atmospheric flow are studied (e.g., Smith, 1979), two different values for the magnitude of the basic flow were used for each of the island distributions. The results obtained were then compared with observed storm cases. It is hoped that this will lead to an improved understanding of many of the island mountain effects, possibly aiding in the forecasting and understanding of storm behavior. Brand (1973, 1974) has shown that these effects, if not properly accounted for, can cause significant error in the forecast of the storm motion.

A brief description of the model, grid system, and the distributions of topography used will be presented in section 2. In sections 3, 4, and 5 the results for each of the three island distributions will be separately discussed in detail. In section 6 these results will be compared with each other, and summarized. Finally, the concluding remarks will be presented in section 7.

2. Model description and experimental design

a. Model description

The triply-nested, movable grid system originally described by Kurihara and Bender (1980) was used for this study. Specific model details are outlined by Tuleya et al. (1984). The grid system for each mesh is the same as used previously in the other landfall simulations performed with the nested grid model and is summarized in Table 1. The model is an 11-level primitive equation model formulated in latitude, longitude and sigma (σ) coordinates, with the outermost domain spanning 37° latitude and 45° longitude. The actual boundary of the outermost domain varied among the various experiments performed and will be given later. The model physics include cumulus parameterization described by Kurihara (1973) with some modifications (Kurihara and Bender, 1980, appendix C), a Monin-Obukhov formulation for the surface flux calculation, and the Mellor and Yamada (1974) scheme (level 2) for the vertical diffusion. Over water, the surface temperature was set equal to 302 K. Similar to the specification in BTK, the land surface temperature (LST) at each point was determined by the following equation:

$$\mathrm{LST} = 298 - \gamma_s z_*. \tag{2.1}$$

Here, γ_s was set equal to 6.7 K km^{-1}, and z_* is the surface height. (See BTK for more details and explanation of this formulation.) Finally, the roughness parameter z_0 was set to 25 cm at all land points.

b. Description of topography

The distribution of z_* for each of the experiments presented was first defined for the entire integration domain at the resolution of the finest mesh (every $\frac{1}{6}$ degree of latitude and longitude). The values of z_* were obtained from the global topography data set prepared by the U.S. Navy's Fleet Numerical Oceanography Center at Monterey, California. In this data set the terrain height provided was the modal height, calculated for the area of each $\frac{1}{6}°$ grid box. Thus individual mountain peaks (or height maxima) were often not resolved even for the very fine resolution used. The

TABLE 1. Grid system of the triply nested mesh model used in each of the experiments.

Mesh	Grid resolution (°)	Time step (sec)	Domain size	
			Longitude (points)	Latitude (points)
1	1°	150	45° (45)	37° (37)
2	$\frac{1}{3}°$	50	11° (33)	11° (33)
3	$\frac{1}{6}°$	25	$3\frac{2}{3}°$ (22)	$3\frac{2}{3}°$ (22)

percent area covered by water was also available and was used to determine the land–sea distribution in each of the experiments. For our case, a particular grid point was considered to be a land point if the percent of water was less than 81%. The values of z_* and percent water for the coarse resolution were then determined by averaging the values of the fine resolution points that were covered by the area of each coarse-mesh grid box. It was assumed that the area mean value of z_* was the appropriate value for the numerical model although it is unclear how subgrid scale topographical features affect the resolvable scale motion.

The first of the three geographical regions that was used in these experiments was an area of the Caribbean (i.e., the Greater Antilles) that included the islands of Hispaniola, Cuba, Puerto Rico and Jamaica. Except for the region containing these islands, the remainder of the land masses of North and South America were not specified in the experimental domain. The other two distributions used were the island of Taiwan and the Philippines. For simplicity, for the island of Taiwan, all other surrounding land areas were removed except both the China coastline and land mass which was replaced by a flat land distribution with a north–south shoreline located 2° longitude from the western most tip of the island of Taiwan. The entire island chain of the Philippines, stretching from 5° to 20°N and also including the island of Taiwan well to the north, was included in the third distribution considered. The outermost integration domain for both the Caribbean case and for the Philippine experiment stretched from 4.5°S to 32.5°N. For the Taiwan case the integration domain stretched from 5.5° to 42.5°N. The island and mountain distributions in the areas through which the tropical cyclones passed are presented in Fig. 1 for all three sets of experiments. It should be pointed out that one of the major differences between the distributions of topography in the Caribbean, and the islands of Taiwan and Luzon is that in the Caribbean region most of the mountain ranges are oriented primarily east–west (parallel to the prevailing flow) while for Taiwan and Luzon most tend to be oriented north–south (perpendicular to the prevailing flow).

c. *Integration procedure*

In a manner similar to BTK, an initially weak vortex was spun up over the ocean, where it quickly intensified to hurricane strength. The vortex was embedded in an easterly zonal flow of constant angular velocity. For all three distributions of topography, two different magnitudes of an easterly zonal flow were used, with initial values of about 5 and 10 m s^{-1} at the center of the integration domain. The initial positions of the vortex varied between each experiment, in order that the positions of the storms at landfall would be approximately the same for each of the two zonal flow experiments.

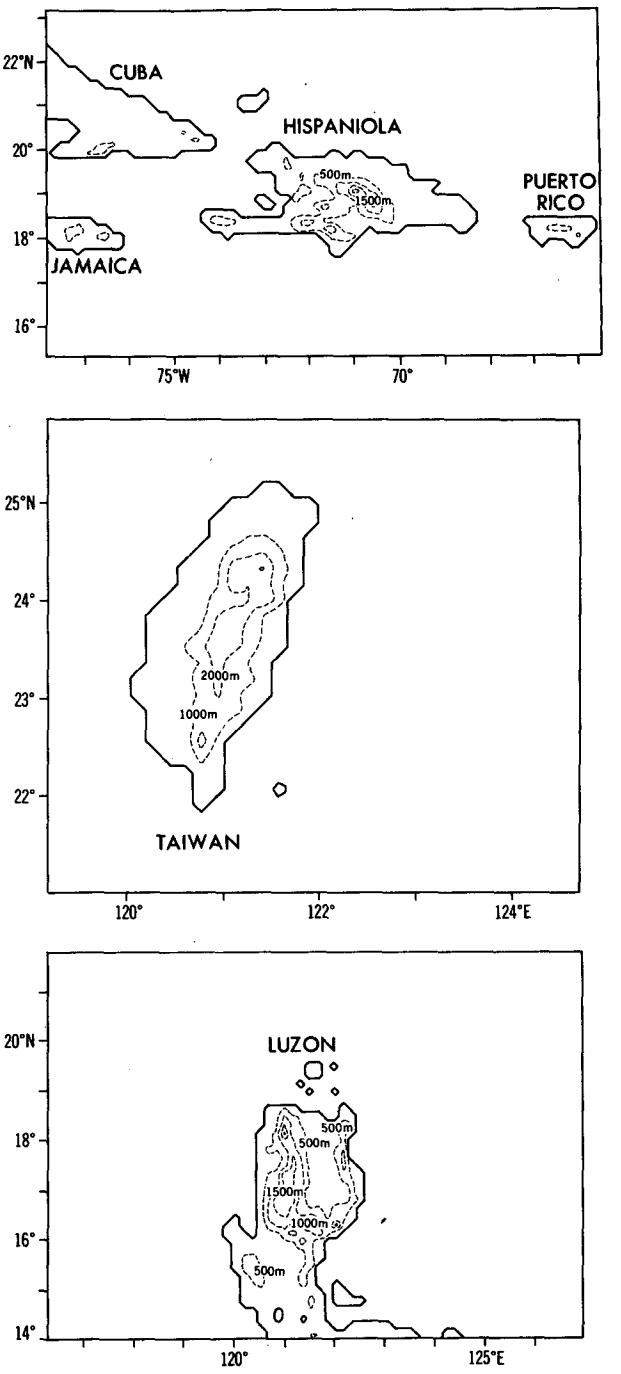

FIG. 1. The topographical distributions used for the three experiments, at the finest mesh resolution (1/6°). Only the regions that were resolved by the innermost grid during the course of the integrations are shown. The topographical heights are contoured at 500 m intervals, for the Caribbean and Luzon, and 1000 m for Taiwan.

The proper position was determined by first running a control experiment with an ocean surface condition at all grid points, for both of the basic flows.

After the storm had reached hurricane strength, the land conditions and topography were implemented into the computational domain. The topography and land condition were inserted at different times for each experiment, so that the entire land distribution would be confined to the coarsest (1°) resolution at that time. Before the integration was resumed, mass and mixing ratio fields were obtained at the new sigma surfaces above the mountains by linearly interpolating between values at the old sigma levels.

Similar to the procedure outlined in BTK, during the course of integration values of z_* and LST at each grid point were kept in a data table for all three mesh resolutions. As the inner grids followed the storm and moved over the island topography, values of z_* and LST which were covered by the coarse resolution were replaced by their corresponding fine mesh values obtained from the table. Thus as the model resolution improved, the shape and height of the topography changed significantly during the course of the integration. For example, as the finer meshes moved over the island of Taiwan, the maximum mountain height resolved by the model increased from 1075 m for the coarse mesh, to 2081 m for the medium mesh and finally 3048 m for the finest mesh. In order to reduce the noise that results from these changes in the mountain shape, if the height (z_*) increased, values of surface pressure (p_*) at the new height were obtained after the grid movement and before the integration resumed, by linearly interpolating between pressure values at the old sigma levels. If the height decreased, the new value of surface pressure was determined over the mountain area by hydrostatically extrapolating down to the new height. For the fields of temperature (T) and mixing ratio (R) the values at the new sigma levels were then obtained by linearly interpolating in pressure between the values at the old sigma levels. Finally, if the pressure at any of the new sigma levels was higher than the pressure of the original lowest model level, linear extrapolation was made downward for T from the lowest two model levels, and R was redefined so that the relative humidity at that sigma level was unchanged. This scheme greatly reduced the noise generated by the movement of the grids over the topography.

Throughout the entire discussion, results for these experiments will be frequently compared with control experiments, run with an identical vortex initially, but with ocean surface conditions at all grid points. An additional set of supplemental integrations will also be discussed which were performed for all three of the island and mountain distributions, with identical easterly flows initially, but excluding the vortex. For these supplemental integrations, the movement of the grids was reproduced to correspond exactly with the grid movements made during the corresponding integrations run with the storm included. A third set of experiments were run for all three of the island distributions, with the vortex again included, but with the surface height (z_*) set to zero and a cool flat land surface condition (LST = 298, z_0 = 25 cm) at all points over the islands. These experiments helped to determine how much of the changes in the vortex structure as it encountered the islands was due to the effect of the land or the effect of the mountainous terrain itself. A summary of all the experiments analyzed in this study is presented in Table 2.

Finally, the sea level pressure over the mountain areas in all of the analysis was reduced hydrostatically from the surface pressure (e.g., Manabe and Holloway, 1975). As mentioned in BTK this yielded a smooth sea level pressure field in most cases.

3. Caribbean Islands

The geography of the Greater Antilles, in the northern Caribbean, consists of four main islands, Hispaniola, Cuba, Puerto Rico and Jamaica, oriented primarily in an east–west direction. The island of Hispaniola is the most mountainous of these islands, with maximum heights resolved by the model of 2498 m, located in the mountain range that transverses the center of the island; peaks exceeding 1000 m are also found in the south central part of the island near the coast. In contrast, the island of Cuba is basically flat, except in the southeast corner of the island. Mountain ranges are found in the center of Puerto Rico and Jamaica,

TABLE 2. Summary of numerical simulations discussed.

Basic experiments

Experiment	Island on which landfall occurred	Approximate magnitude of initial easterly basic flow (m s^{-1})
Exp. C5	Hispaniola, Cuba	5
Exp. C10	Hispaniola, Cuba	10
Exp. T5	Taiwan	5
Exp. T10	Taiwan	10
Exp. L5	Luzon	5
Exp. L10	Luzon	10

Supplemental experiments

Type	Description
Ocean controls	5 and 10 m s^{-1} basic flow and vortex. Ocean condition everywhere (LST = 302, z_* = 0, z_0 = Charnock's relation.) Run for each of the six basic experiments.
Basic flow simulations	5 and 10 m s^{-1} basic flow with vortex not included. In particular, experiment run with Taiwan topographical distribution and 5 m s^{-1} basic flow is referred to as Exp. TZF.
Flat land simulations	Landfall simulations with 5 m s^{-1} basic flow and vortex. Flat land condition everywhere over islands (LST = 298, z_* = 0, z_0 = 25 cm). Run for the three topographical distributions.

with the maximum peaks resolved by the model of 640 and 764 m respectively, for these islands.

In this section two primary experiments will be discussed: Exp. C5 (Caribbean, 5 m s^{-1}) which was integrated to 126 h and Exp. C10, integrated to 84 h.

a. Storm track and motion

In Exp. C5, the topography and land conditions were inserted into the integration domain at 26 h, when the islands and the topography were still entirely confined to the outer mesh. The storm track and the sea level minimum pressure for this experiment as well as the all-ocean control experiment is shown in Fig. 2. The storm began to gradually accelerate and veer to the left as it passed south of Hispaniola, with landfall occurring on the extreme southern tip of the island at about 88 h. Its position at that time was about 70 km west-southwest of the ocean control. Minimum sea level pressure at landfall was 979 mb. At this point the storm's movement underwent a noticeable acceleration with a sharp deflection to the northwest as it crossed the western end of the island. During this time the storm continued to rapidly decay to tropical storm strength, crossing the western coast at 94 h. Once over the ocean environment the storm again intensified reaching hurricane strength by 102 h with landfall occurring on the southern coast of Cuba at 108 h. By this time the storm was about 120 km northwest of the storm in the ocean-only control case. A small northward deflection again occurred as it passed over southern Cuba. Toward the end of the integration (120 h), the storm was located about 150 km north-northwest of the control simulation.

Similarly, the storm track for the simulation run with a 10 m s^{-1} initial easterly flow (Exp. C10) is presented in Fig. 3. Once again the storm's translational speed increased slightly as the storm approached Hispaniola. In this simulation, landfall occurred at 62 h with a minimum sea level pressure of 980 mb. No significant difference in minimum central pressure compared to the ocean control case occurred until about 59 h, about 3 h before the storm crossed the southern tip of the island. After landfall the storm accelerated, similar to Exp. C5, with a deflection in the storm track to the northwest once again. Rapid weakening to tropical storm strength occurred at this time, with the storm filling 17 mb during the 6 h period after landfall. The storm eventually regained hurricane strength over the ocean, before landfalling on Cuba. Toward the end of the integration (80 h) the storm was located about 105 km to the northwest of the storm in the ocean-only control experiment.

The most noticeable feature of both of these experiments was the sharp turning of the storm to the northwest as it passed over Hispaniola. For example, in Exp. C5 the average north–south component of the storm's translational speed increased from 2.1 m s^{-1} when the storm was well east of Hispaniola to 7 m s^{-1} during the period from 90 to 94 h when the storm was moving across the southwest portion of the island. In order to help understand this deflection in the storm path, a

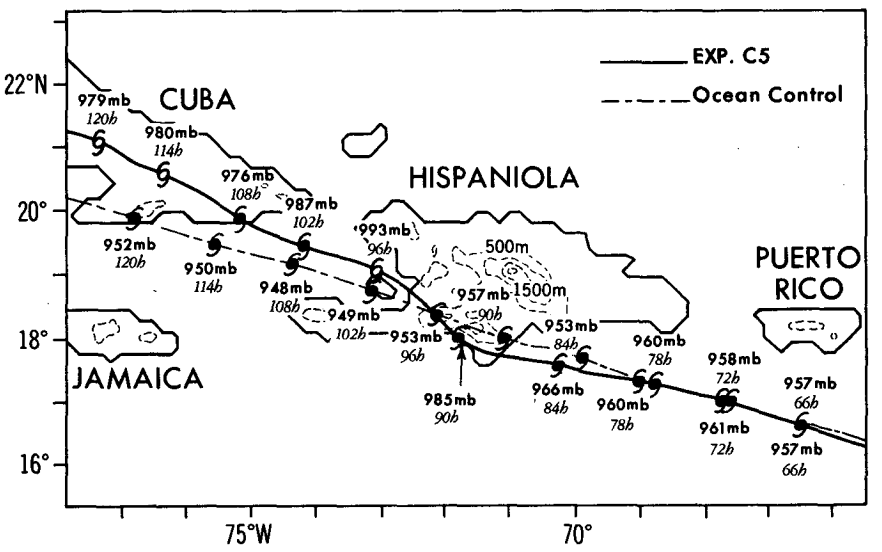

FIG. 2. Storm tracks for Exp. C5 (solid line) and the ocean-only control case (dashed line). The Caribbean island distribution used in Exp. C5 is shown. The mountain heights are contoured with a thin dashed line at 500 m intervals, with the shoreline indicated by a thick solid line. Storm positions defined by the sea level pressure field, are plotted every 6 h and indicated by a tropical cyclone symbol, with the storm's minimum sea level pressure indicated.

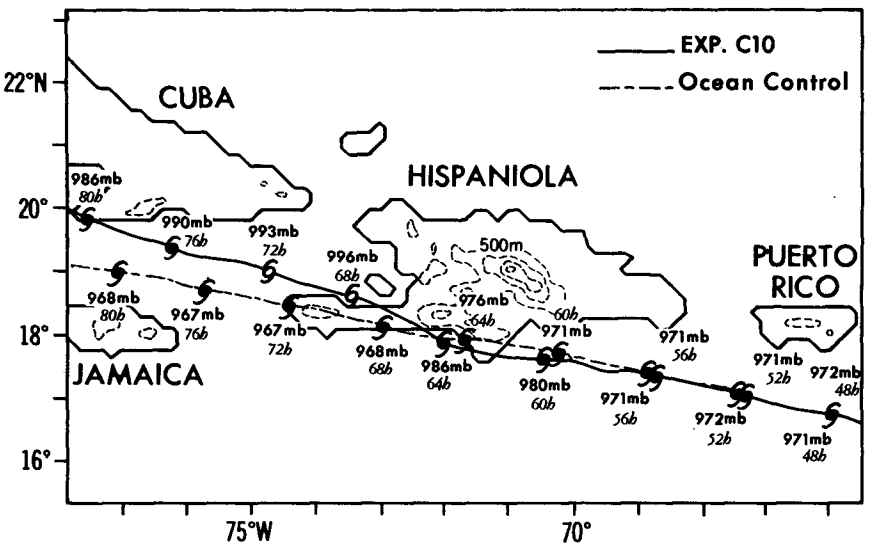

FIG. 3. As in Fig. 2 but for Exp. C10 and the 10 m s^{-1} ocean-only control experiment. Also, storm positions are plotted every 4 h.

supplemental experiment was performed for the same distribution of topography and identical easterly flow as Exp. C5 (~5 m s^{-1} initially) but excluding the vortex. The numerical results indicated that southerly flow did indeed exist throughout much of the atmosphere in the southwest corner of the island, where the storm eventually veered north. The values of the southerly wind component were about 2 to 8 m s^{-1}, with maximum values of about 10 m s^{-1} found between 2 and 8 km. Weak southerlies (~1 to 2 m s^{-1}) extended to about 100 km north of the island, with weak northerlies extending from the western Hispaniola coast to about 300 km westward. Kasahara (1966) indicated that, for easterly flow over an isolated mountain region (which is a first order approximation to this experiment), modification of the flow field occurs primarily in the vicinity of the obstacle. This tended to occur in our case. The analysis of the flow field also indicated that the easterly component of the wind in the middle atmosphere increased by several meters per second over Hispaniola, possibly contributing to the acceleration of the storm in the east–west direction that occurred in this region.

As the storm center in Exp. C5 veered north between 90 and 96 h, the outer region of the storm system moved with a smaller north–south translational speed than the interior of the storm. This caused the pressure field to become somewhat distorted. For example, if we consider the 1008 mb surface pressure contour, located about 250 km radius from the storm center at 90 h, to be representative of the storm's larger-scale pressure envelope, we find that the position of the storm center relative to the position of the center of the envelope shifted north during this time. At 90 h the storm center was located about 38 km to the north of the center of the envelope, increasing to 83 km by 96 h. After 96 h as the storm center once again moved in a west-northwest direction the storm's interior became better centered within the pressure envelope. By 100 h its position relative to the center of the envelope became roughly the same as the position at 90 h.

The storm tracks of three observed tropical cyclones that passed through this region are presented in Fig. 4. We see that all three of these observed storms exhibited a noticeable northerly shift in their track near the island of Hispaniola. It is difficult, however, to determine if the abrupt deflection of David and Frederic to the north, which occurred further to the east than our model storm, was chiefly a result of the island topography or interactions with the large-scale flow field. Hurricanes Inez and David also underwent accelerations in their motion as they crossed Hispaniola, with rapid weakening occurring during this time, similar to our model storms.

It should be pointed out that not all storms that passed near to Hispaniola actually have exhibited a northward perturbation in their track. For example, some of the storm tracks have moved straight across the island with one example (Beulah, 1967) being deflected southwest after passing near to Hispaniola. These differences indicate the large variability that the island effects may have with the different storm structure and steering flow that is present.

Finally, a second supplemental experiment was also performed with the same vortex and 5 m s^{-1} initial basic flow, but with the topographical distribution of each island replaced by a cool flat land surface (i.e., LST = 298, z_0 = 25 cm, and $z_* = 0$ everywhere over

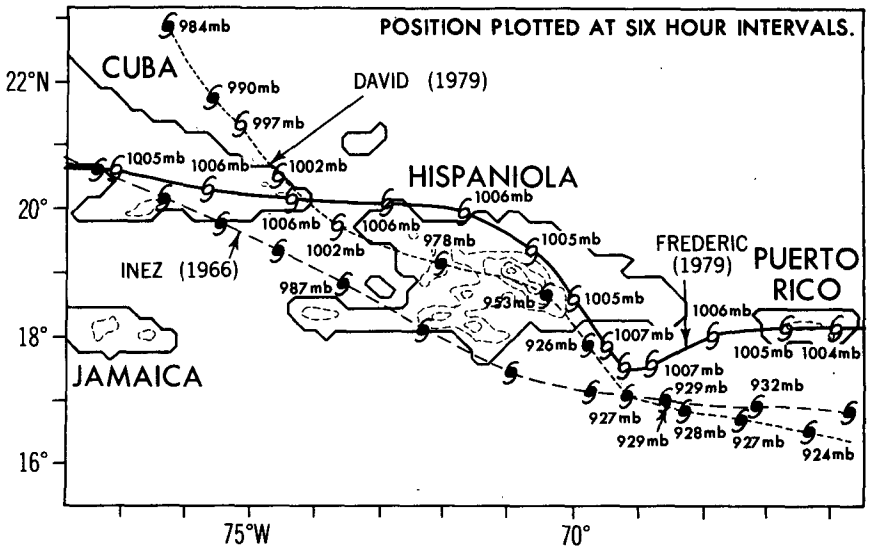

FIG. 4. Storm tracks for three observed tropical cyclones, David, Frederic and Inez. The Caribbean island distribution used in the model simulations is shown. Storm positions were plotted at 6 h intervals, with the storm's minimum sea level pressure indicated where the data were available. (See Fig. 2 for more details.) The storm tracks were obtained from the Monthly Weather Review's Atlantic Hurricane Summaries (i.e., Hebert, 1980; Sugg, 1967).

land). As mentioned before, this experiment was run to determine how much of the storm behavior was a result of its interaction with the land condition, apart from any orographic effect. During the first part of the integration, the position of the vortex was very near the vortex position in the ocean control. However two hours before landfall, the storm began to turn slightly further north, reaching Hispaniola about 18 km north of the ocean control. Analysis indicated that there was enhanced coastal convergence over the land in this region, just prior to landfall. Also, the storm had undergone some weakening prior to this time. When the storm left the western side of the island it was located about 30 km north of the ocean control. Thus the northerly movement of the storm in this experiment (75 km) was considerably less than was observed in Exp. C5 (143 km) during passage over a similar longitudinal span of the island.

b. Structural change and storm decay

As was mentioned in the previous subsection, the storms in both Exp. C5 and Exp. C10 underwent noticeable decay before landfall onto Hispaniola. Since analysis results of BTK indicated that the reduced moisture supply was the primary cause of the enhanced storm decay as it interacted with the model topography, the low-level moisture fields in Exp. C5 were examined (Fig. 5). As the storm passed south of Puerto Rico, slightly drier air originating from the mountain range in the center of the island was advected into the storm domain. Our analysis indicated that much of this drier air originated in the regions east of Puerto Rico and was forced up the mountain range in the center of the island. Light precipitation occurred on the upwind side of the mountains as these air parcels were advected onto the island and ascended the mountain slope. Gradual weakening of the tropical cyclone began after 78 h and continued until about 84 h, when, with the storm about 50 km south of the coast of Hispaniola, considerably drier air from the mountains of the island began to be advected into the storm region. Since the actual trajectories of these air parcels is quite complicated, it is difficult to precisely determine the source of this dry air. Cross sections through the mountain range seemed to indicate that some of the dry air originated from subsidence above the mountains as well as from downslope flow near the mountain top. In some cases, enhanced precipitation was again occurring on the upwind side of the mountains, serving to dry the air that eventually descended to the lower levels and was drawn into the storm circulation.

The advection of the dry air into the storm caused a rapid weakening of about 3 mb h^{-1} in the central surface pressure which continued until the storm finally approached the western coast of Hispaniola at 94 h. The storm decay then leveled off with reintensification beginning about 2 h later as the storm began passing over the ocean environment again. We see from Fig. 5 that during this redevelopment period moist air which was advected into the area between Cuba and Hispaniola (96 h) and from the south (102 h) reached the

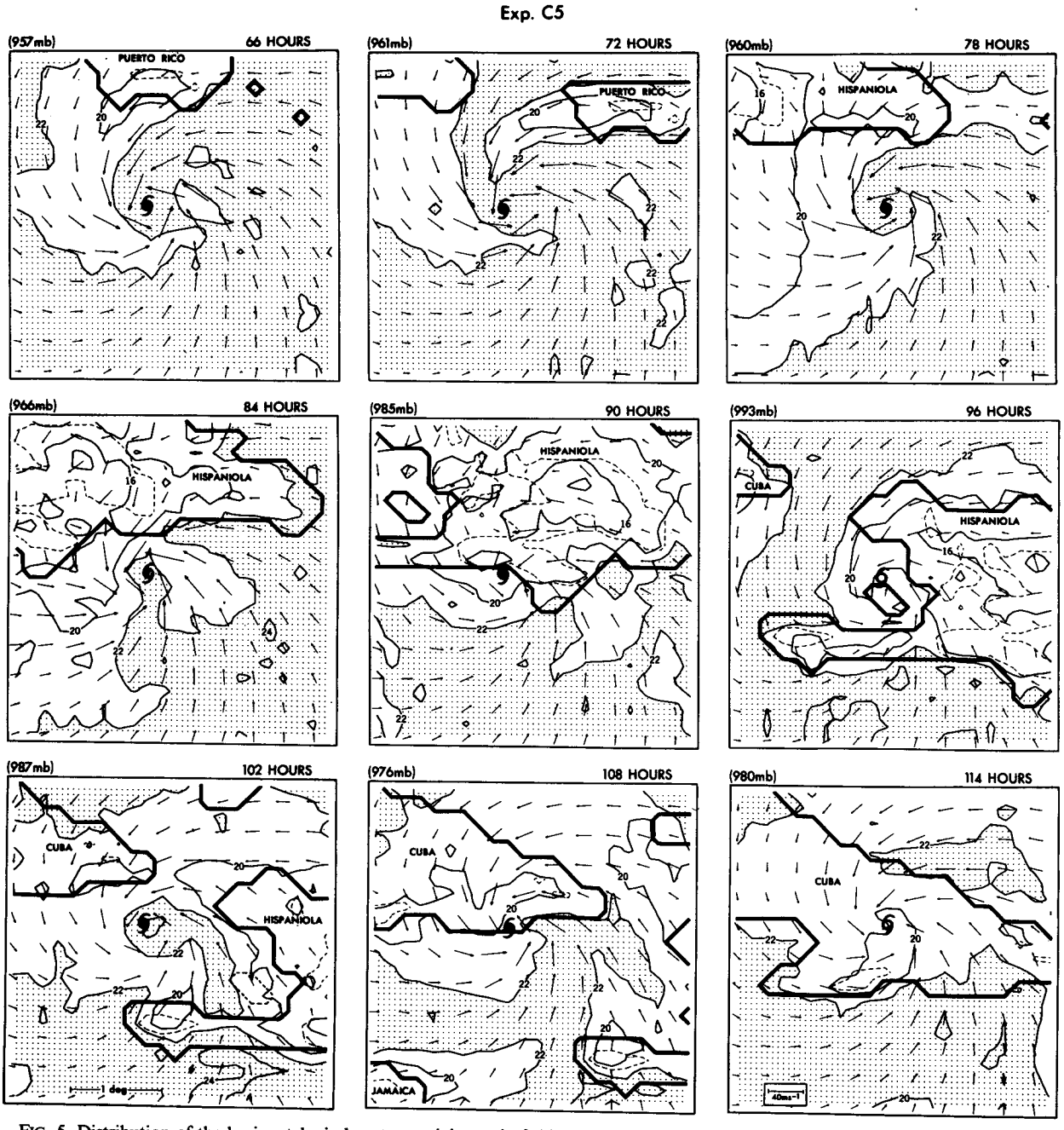

FIG. 5. Distribution of the horizontal wind vectors, mixing ratio fields (solid line) at model level 11 (σ = 0.992) in the finest mesh for Exp. C5. Maps are shown at 6 h intervals. The shoreline is indicated by a thick solid line with the 500 m topographical height contoured (dashed line). Wind vectors are plotted at every other grid point. The areas with mixing ratio greater than 22 g kg^{-1} are shaded. The storm center, defined by the sea level pressure field, is indicated by a tropical cyclone symbol. Finally, the storm's minimum sea level pressure at each time interval is given at the upper left of each frame.

storm region. After landfall over the island of Cuba the storm weakened once again; however, the proximity of the ocean environment to the storm center caused the weakening to be small. These results clearly show the high correlation between the intensity change and the moisture supply.

During the passage of the storm over the island of Hispaniola, the storm system maintained vertical coherence with height, in contrast to Exp. M of BTK which exhibited a vertical tilt of the circulation centers. In Exp. M the disorganization of the storm system with height appears to have enhanced the decay of the storm.

When analysis was made for the experiment run with a flat land condition and 5 m s^{-1} basic flow, it indicated that the weakening of the storm was much less than found in Exp. C5 as the storm passed over and just south of Hispaniola. For example, the storm's minimum sea level pressure as it left the island was 979 mb compared to 993 mb for Exp. C5.

4. Taiwan

The topography of the island of Taiwan consists of a narrow but very steep mountain range (Central Mountain Range). This range stretches much of the length of the island, and is located very close to Taiwan's eastern coast. Although many of its peaks tower to well over 3000 m, the mountain heights resolved by our fine mesh topography reached above 3000 m in only one region (3048 m maximum), located at the northern part of the island. Still, mountain heights of over 2500 m were located in a large area in the center of the island in our model topography. The entire length of the island stretches about 3° latitude with the average width of the Central Mountain Range less than 100 km.

In this section three experiments will be discussed which used this topographical distribution: Exp. T5 (Taiwan, 5 m s^{-1}); the supplemental experiment Exp. TZF (Taiwan, zonal flow only); and Exp. T10. The length of the integrations for Exps. T5 and T10 were 92 and 88 h, respectively.

a. Storm track and motion

Once again the island topography was inserted into the model domain when the island was entirely confined to the coarse mesh (44 h for Exp. T5 and 52 h for Exp. T10). The storm track for the case of Exp. T5 is shown in Fig. 6. Well upstream of Taiwan the storm's forward motion decreased relative to the control. However, as the storm approached to about 200 km from the island it began to curve to the northwest and accelerate. By 84 h the storm speed accelerated to about 12 m s^{-1}, landfalling on the extreme northern tip of Taiwan an hour later.

The storm motion agrees well with some observed storms, as can be seen in Fig. 7. All of these storms had a mean translational speed well upstream of the island of 5 m s^{-1} or less. Besides being cyclonically deflected around the northern end of the island, all three storms exhibited a noticeable acceleration in speed as they approached the island. One hour before landfall, the average translational speed of the three storms was 11.6 m s^{-1}. Our storm motion in Exp. T5 is also in general agreement to that which was obtained by Chang (1982) in his numerical simulation of the passage of a tropical cyclone that was embedded in a 5 m s^{-1} initial zonal flow over an island mountain range. However, in his case the northward deflection was not as great as we found, and the storm traveled over the northern part of the mountain range. The differences may have been partly due to the coarser model resolution as well as the distribution of topography he used, which consisted of an idealized mountain range with maximum height of 2000 m and width of about 240 km. Thus, his mountain range did not create as much of a barrier to the flow as the more realistic topography used in our experiment.

A supplemental experiment without the vortex (Exp. TZF) was performed in order to help explain the northward movement of the storm. The basic flow field in the lower 4 km indeed curved to the northwest in this simulation (Fig. 8) well upstream of the island, with the maximum southerly wind component centered at about 2 km (Fig. 8, top). However, the storm's fast translational speed (e.g., a north–south component of over 8 m s^{-1} between 81 and 84 h) was too large to be explained by the magnitude of the wind in Exp. TZF. This can clearly be seen in Fig. 9. From this figure we see that the computed low-level average wind speed surrounding the storm in Exp. T5 was very well correlated with the actual storm translational speed of Exp. T5. The correlation with the mean wind at higher levels was not as good, although significant increase of the mean flow still existed to about 500 mb. This indicates that the storm was apparently advected by the accelerated mean flow that primarily existed at the lower levels. Thus, the deflection of the storm to the north with the subsequent acceleration in speed was partly due to the influence of the mountain range on the basic flow, with an additional interaction of the storm circulation itself with the mountain range. As the storm began to approach the island the winds southwest of the storm center acquired a more southerly component, and the winds northwest of the storm turned more northeasterly from northerly (see Fig. 12). It is speculated that this type of topographical effect contributed to the change in the environmental flow, leading to the deflection and acceleration of the storm. Chang (1982) in his simulation also observed that the interaction between the terrain and the tropical cyclone caused strong easterlies to develop north of the island, accelerating the storm in his case. He indicated that movement of the tropical cyclone near the mountain was a result of the low-level rather than the middle tropospheric flow.

A comparison was also made between the all-ocean control and an experiment in which the topography of Taiwan was replaced by a cool flat land surface. In this case there was no northward deflection of the storm, with no significant change in the positions of the storms in the two experiments. This confirms that the northward deflection of the storm in Exp. T5 was solely a topographical effect. Also, in this supplemental experiment there was no storm decay east of the island, al-

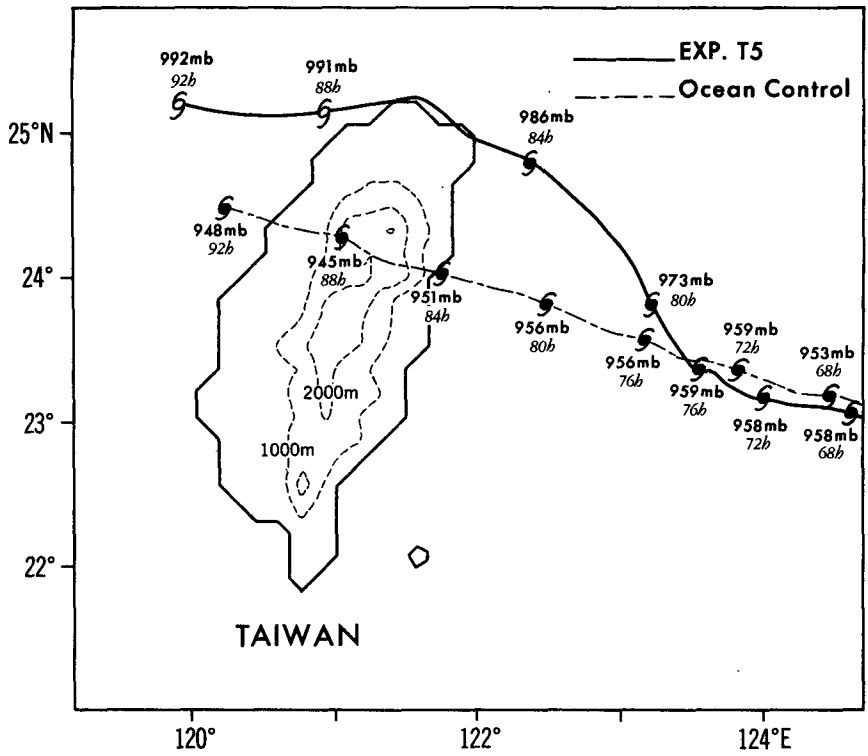

FIG. 6. Storm tracks for Exp. T5 (solid line) and the ocean-only control case (dashed line). The topographical distribution used in Exp. T5 is also shown with the heights contoured at 1000 m intervals. Storm positions are plotted at 4 h intervals. (See Fig. 2 for more details.)

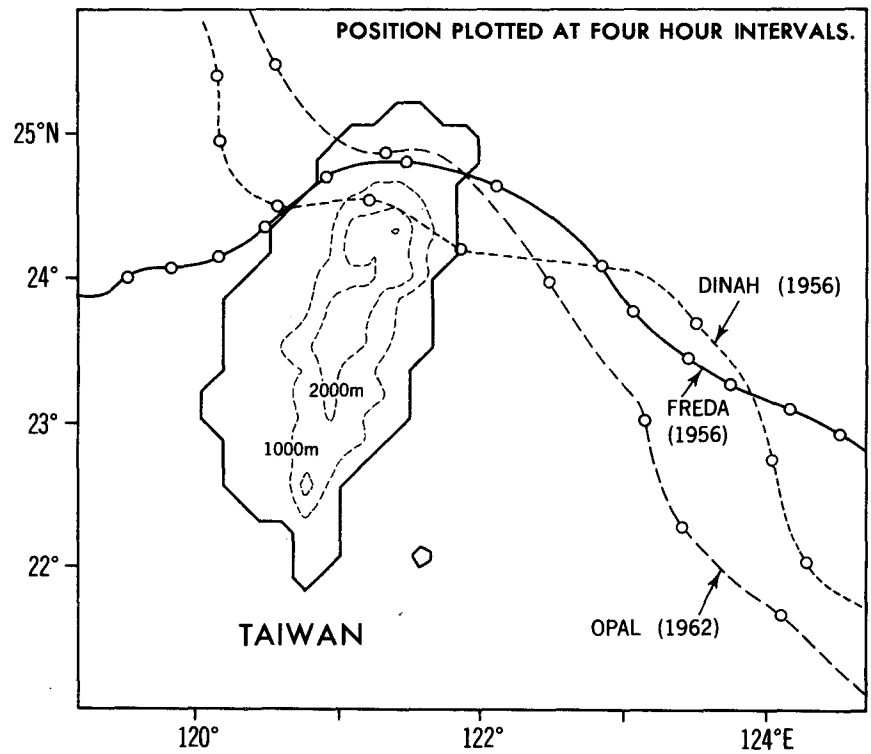

FIG. 7. Storm tracks for three observed tropical cyclones that landfalled on Taiwan, namely, Dinah, Freda, and Opal, which exhibited a significant northward deflection (Wang, 1980). The Taiwan island distribution used in the model simulations is shown. Storm positions at 4 h intervals are indicated by open circles.

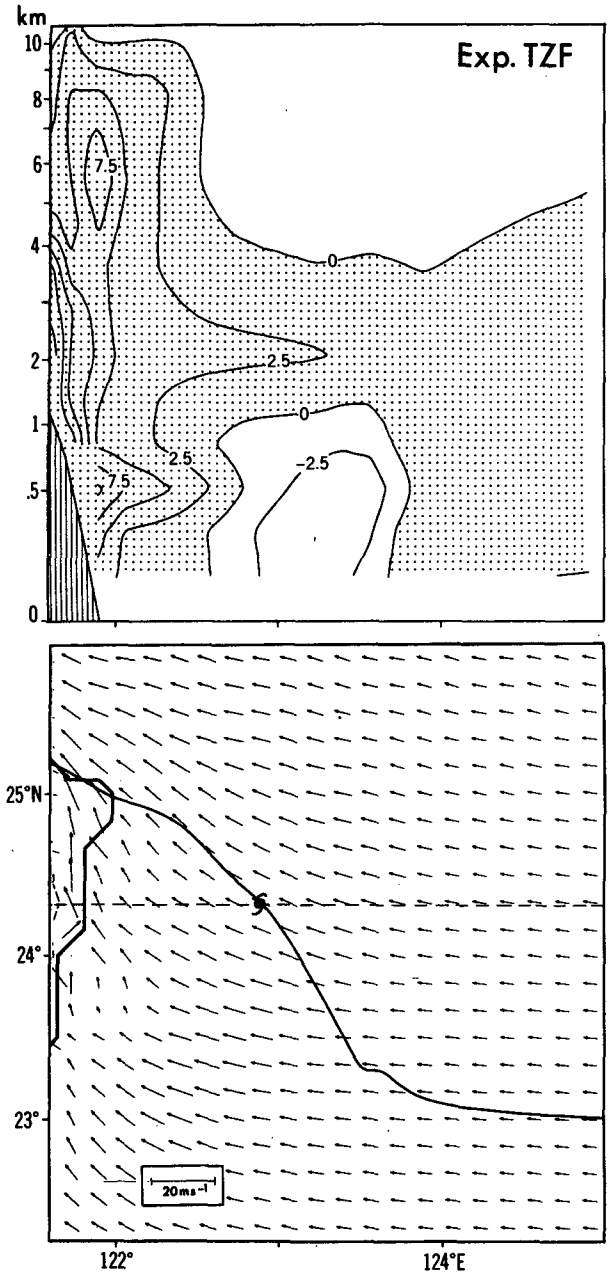

FIG. 8. East–west vertical cross section (upper figure) through 24.25°N at 82 h for Exp. TZF. The meridional component of the flow is contoured (m s^{-1}), with southerly flow shaded. The vertical coordinate for this cross section is the square root of height in meters. (See Fig. 11 of BTK for more details of this coordinate system.) The actual height (km) is presented on the left side of the map. Horizontal distribution of the wind vectors (bottom figure) for this same time period is also shown at the 2 km height. The storm track for Exp. T5 is plotted here for comparison. The storm position at 82 h is also indicated. The latitude through which the cross section was taken is indicated by a dashed line.

though the storm weakened several millibars as it transversed Taiwan.

The storm track for Exp. T10 is presented in Fig. 10. In this case, the storm was not deflected to the north before reaching Taiwan, and landfall occurred on the central portion of the island. A secondary surface pressure center eventually formed on the western side of the mountain range and drifted slowly to the northwest. Within the next hour a third low formed just off the western coast, and moved away from the island. The above sequence of the development of secondary surface pressure centers will be looked at in detail in subsection c.

When a supplemental experiment was run without the storm, it was found that in the absence of the vortex, the 10 m s^{-1} easterly flow did not produce any southerly wind component upstream of the island; this is in contrast to the simulation run with the 5 m s^{-1} easterly flow mentioned before.

Several examples of storm tracks without significant deflection upstream of the island can be found, as summarized by Wang (1980). The storms that moved basically in an east–west direction in his study generally exhibited a faster east–west translational speed well upstream of the island than those that deflected to the north or to the right of the storm track. This was in agreement with the movement of our storm in Exp. T10. Some examples of this type of storm track are shown in Fig. 11. The three storms shown here had an average east–west translational speed of 9.8 m s^{-1} well upstream of the island, in contrast to 4.5 m s^{-1} for those presented in Fig. 7.

From his numerical results Chang (1982) concluded that storm intensity may also have a significant impact on a storm's motion and behavior. However, since both Exps. T5 and T10 were of comparable intensity well upstream of Taiwan, we could not confirm the importance of this effect.

b. Storm decay

For both Exp. T5 and Exp. T10 the storm began to decay upstream of the island. For Exp. T5 the decay began about 10 h before landfall. During this time the maximum low level winds decreased from about 50 to 33 m s^{-1} at landfall, with a value of about 27 m s^{-1} as the storm left Taiwan. The minimum sea level pressure at landfall was 988 mb with the storm's central pressure filling 33 mb during the 12 h before reaching the island. Brand and Blelloch (1974) in their statistical study of 22 typhoons that eventually landfalled on the island of Taiwan indicated that those storms, which exhibited an average east–west translational speed of about 5 m s^{-1} well upstream of the island, began to show significant decay about 12 h before they reached the island. In these cases the average maximum surface winds decreased from about 52 to 40 m s^{-1} at landfall, with a value of about 32 m s^{-1} as the storms crossed the island's western coast. In contrast, in the numerical simulation by Chang (1982) the reduction of the maximum surface winds ended before landfall, with the surface winds increasing again during passage of the storm over

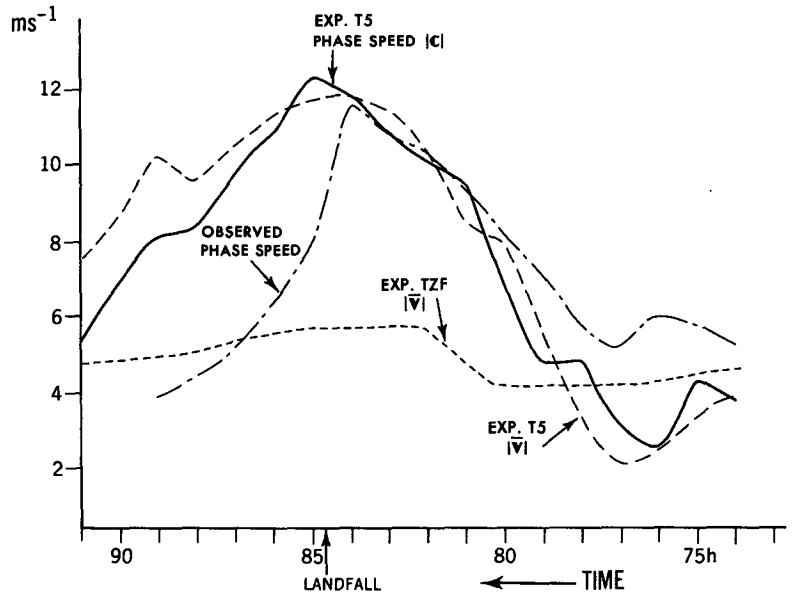

FIG. 9. Time series of the storm's translational speed (|C|) for Exp. T5, as well as the average wind speed ($|\bar{v}|$) calculated for the entire inner mesh at model-level 7 (about 2 km above the surface over the ocean) for the simulations with the storm (Exp. T5, long dashed line) and without the storm (Exp. TZF, short dashed line). In this figure time increases to the left. For comparison, the average phase speed for the three observed storms (long dashed, dotted line) shown in Fig. 7 is also plotted relative to the time of landfall.

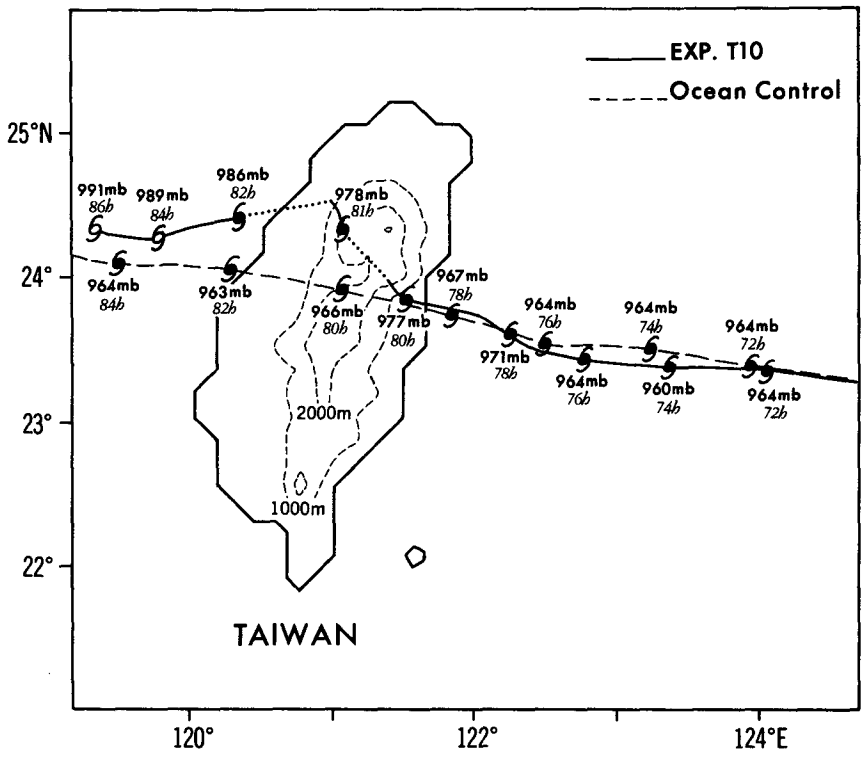

FIG. 10. As in Fig. 6 but for Exp. T10 and the 10 m s^{-1} ocean-only control experiment. Also, storm positions are plotted every 2 h unless otherwise indicated. (See Fig. 2 and Fig. 6 for more details.) When the track was not continuous, the storm's surface positions were connected by a dotted line.

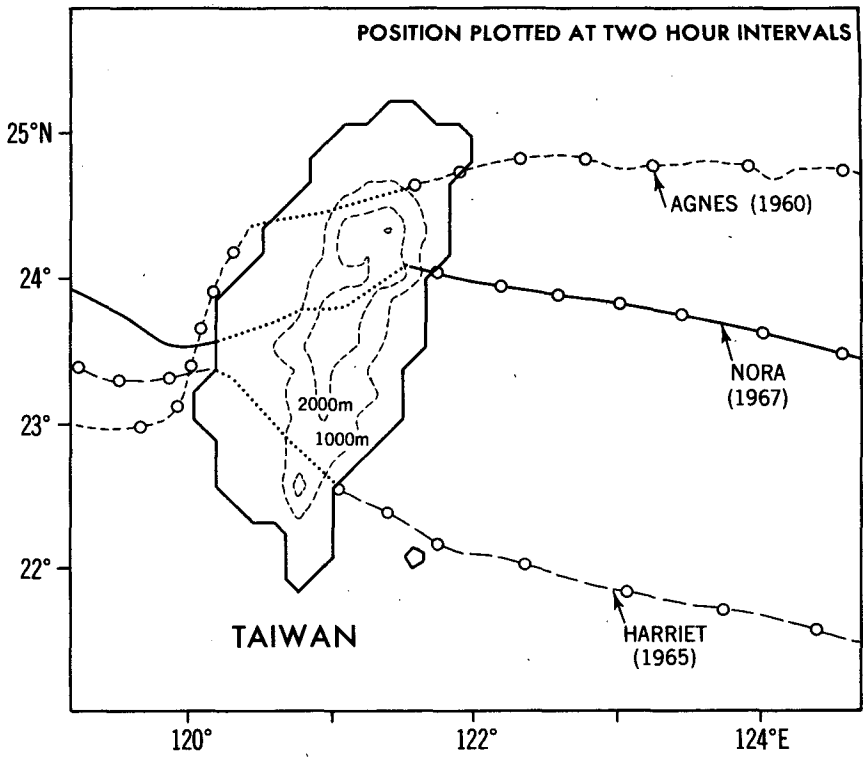

FIG. 11. The storm tracks of three observed storms (Harriet, Nora, and Agnes) (Wang, 1980) that did not exhibit a significant northward deflection when they landfalled on Taiwan. Storm positions plotted at 2 h intervals are indicated by open circles. When the track was not continuous, the storm's surface positions were connected by a dotted line.

the island. For Exp. T10 the storm did not begin to significantly decay until about 3 h before the storm reached the eastern shore of Taiwan. The minimum sea level pressure at landfall for this case was 976 mb, with the storm's central pressure filling 22 mb during the 6 h period centered at the landfall time.

In order to explain the reasons for the upstream decay of the storm, moisture fields are shown in Figs. 12 and 13 for both experiments. For the weaker easterly flow (Fig. 12) we notice that drier air originating from the mountainous region of Taiwan began to interact with the storm circulation about 12 h before landfall, i.e., 73 h, when the storm was about 230 km from the coast. Much of this air originated from near or above the mountain top, and was transported down the mountain as the storm circulation approached the island. The transport of air to the surface from aloft was aided locally by regions of very strong subsidence associated with the steep topography. Hence, the storm began to rapidly decay, filling about 17 mb in the next 6 h.

Figure 12 also indicates that as the dry tongues spread over the ocean, some moistening of the dry air occurred as a result of the evaporation from the ocean surface. It should be pointed out, however, that the effect of evaporation of rain droplets which is not included in our model may also modify the moistening rate.

For Exp. T10 (Fig. 13) we see that the advection of drier air toward the storm circulation was retarded because of the stronger easterly component of the wind. Also, since the storm in Exp. T10 was moving faster there was less time for the dry air to reach the storm region. Hence, significant storm decay did not begin until the storm was about 110 km east of the coast (about 3 h before landfall, i.e., 76 h).

As the storm in Exp. T5 approached Taiwan, the circulation centers became vertically tilted with height, beginning at about 80 h. By landfall, the maximum vertical tilt between 2 and 8.1 km heights was about 35 km. As mentioned in section 3, a similar feature occurred in the storm in Exp. M of BTK, particularly as it descended the mountain range. This added to the disorganization of the entire storm system in both experiments, and could also have contributed to the decay of the storm in Exp. T5 in the period beginning about 5 h before landfall. For the case of Exp. T10, no tilting of the circulation centers with height was observed until right before landfall (see Fig. 14).

c. Formation of the secondary lows

One of the most interesting features of Exp. T10 was the formation of secondary surface pressure centers on the western side of the island as the storm encountered

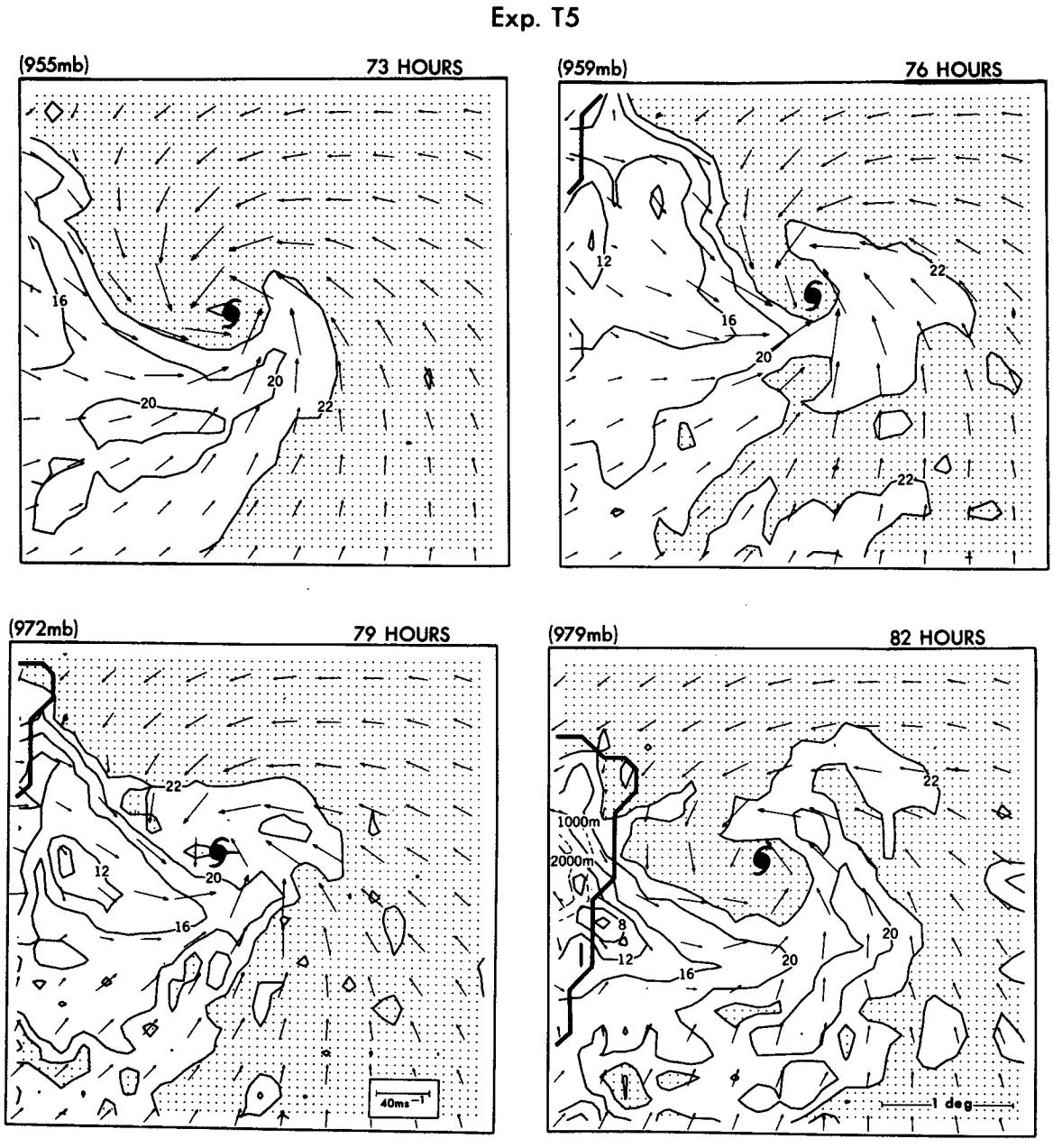

FIG. 12. Distribution of the horizontal wind vectors, mixing ratio field (solid line) at model level 11 (σ = 0.992) and topographical heights (dashed line, 1000 m contour) in the finest mesh for Exp. T5. The maps are shown for four time periods at 3 h intervals when the storm was east of Taiwan. (See Fig. 5 for more details.)

the mountain barrier. As our model storm encountered the mountain range at 80 h (Fig. 14, system A), two other surface lows subsequently formed (systems B and C). A second circulation center in the lower atmosphere (2 km) also formed on the western side of the mountain and subsequently moved slowly north and then northwest. It finally became coupled with surface system C at 82 h. In contrast, the path of the circulation center at the upper level remained continuous as it crossed the island mountain range undergoing acceleration in its translational speed without significant deflection.

Figure 15 shows an hourly sequence of surface features during the period in which the secondary lows formed. At 79 h, as the primary storm center (system A) was nearing the coast, a second surface low, with an associated increased low-level cyclonic vorticity, had already formed in the region where very strong adiabatic descent of winds down the mountain slope was

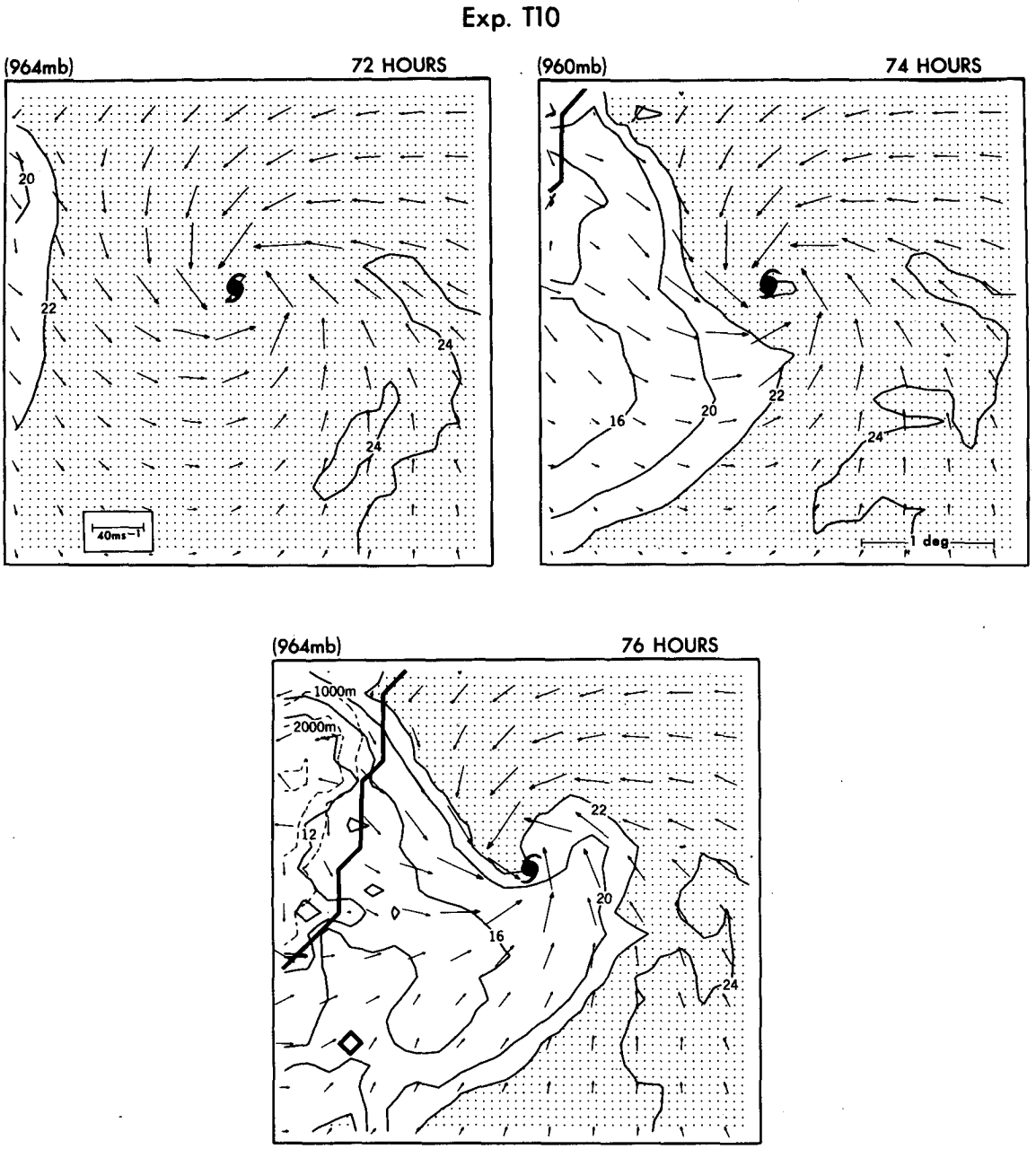

FIG. 13. As in Fig. 12, except for Exp. T10. The longitudinal position of the storm at the upper left hand frame is the same as the longitudinal position of the storm at the upper left hand frame of Fig. 12. The maps are shown at 2 h intervals.

occurring. By 80 h the minimum central surface pressure of the secondary low (system B) had dropped to below 990 mb, with an area of hurricane force winds associated with it. By 81 h the primary center (system A) had disappeared, and air from most sides of the island was advected into system B. Note that the center of system B had remained stationary during this time. There were indications of a third system (system C) beginning to form just off the coast near the location of the circulation center at 2 km. During the next hour system B moved slowly to the northwest and weakened, while the circulation associated with system C increased. By 82 h, hurricane force winds had jumped entirely to system C located off the coast. As this system continued to move away, system B continued to decay.

The actual sequence and details in the structural change of the tropical cyclones encountering Taiwan's island barrier vary from storm to storm (e.g., Wang, 1980). Thus it is impossible to generalize this particular sequence found in Exp. T10 to formation of secondary

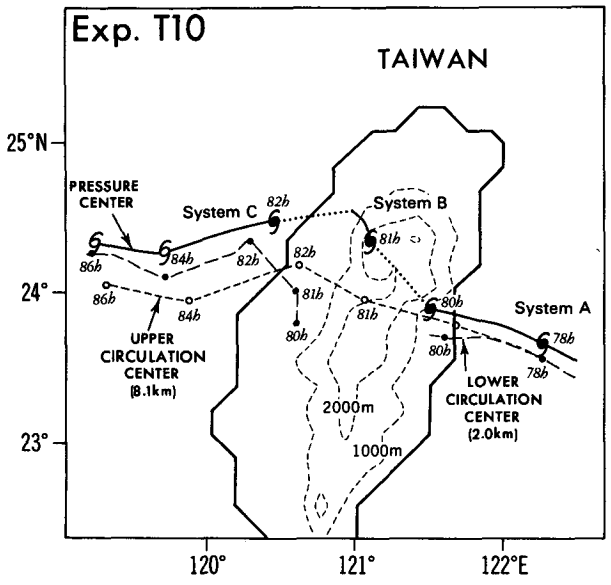

FIG. 14. Tracks and positions of the storm's minimum sea level pressure (solid line and tropical cyclone symbol), and the center of circulation of the wind field at the 2 km (long dashed line and closed circle) and 8.1 km (short dashed line and open circle) heights for Exp. T10. The primary surface low is identified in the figure as system A. The second surface low is identified as system B, with the third surface center that formed off the coast identified as system C. When the track was not continuous, the storm's surface positions were connected by a dotted line. The Taiwan coastline is indicated by a thick solid line with the topographical heights contoured (dashed line).

lows in general, although it does appear to bear similarity to some observed storms (e.g., Typhoon Louise, 1959).

As system A approached the coast, hurricane force winds were forced up Taiwan's steep eastern slope (Fig. 15). This caused a large enhancement of storm precipitation north of the storm center (Fig. 16), with values of total storm rainfall exceeding 25 cm (27.6 cm maximum). As system B formed on the west side of the mountain range, strong upslope flow began to occur in the area south of this system. Thus, an enhancement of precipitation occurred in this region as well. This seemed in good agreement with results obtained in the previous study (see Fig. 6 of BTK) and agrees in general with observed precipitation distributions for landfalling tropical cyclones in mountainous regions (e.g., Brunt, 1968; Hamuro et al., 1969).

5. Luzon

The northernmost island of the Philippine Island chain, called Luzon, has a very mountainous topographical distribution, especially on the northern half of the island in which our model tropical cyclones crossed. Two distinct north–south mountain ranges span this section of Luzon: the first located near the eastern coast (Sierra Madre), and the second and steeper range (Cardillera Mountains) spanning the western part of the island. Many of the peaks in this mountain range tower over 2000 m high, with maximum heights resolved by the models of 2134 and 2042 m located in the north and central parts of the mountain range, respectively. Between these two ranges is a broad valley. The average width of northern Luzon is over 210 km, making it considerably wider than the island of Taiwan.

The two experiments to be discussed are Exp. L5 (Luzon, 5 m s^{-1}) and Exp. L10, integrated to 92 and 62 h respectively.

a. Storm track and motion

The topography of Luzon and the land conditions were inserted into the integration domain at 16 h for Exp. L5 and 12 h for Exp. L10. For Exp. L5, the tropical cyclone reached the coast of Luzon at about 65 h (Fig. 17). Upstream of the island the storm was deflected slightly to the left relative to the ocean control and underwent a small deceleration. As the storm continued to approach the island its direction began to shift to the northwest about 2½ h before landfall and it rapidly weakened. By landfall the storm also began to move with an accelerated speed (from 5 m s^{-1} at 62 h to about 7.5 m s^{-1} at 66 h), reaching the center of the island at 68 h as a tropical storm. At this time the surface pressure field became quite distorted. The surface pressure center reformed on the western side of Luzon, slowly moved toward the north, and eventually moved out over the ocean in a northwest direction. As the storm continued to move over the ocean west of the island, its translational speed began to again accelerate, reaching a maximum of about 8.2 m s^{-1} at 80 h. The profile of the storm's translational speed seemed to compare fairly well qualitatively with Brand and Blelloch's (1973) statistical study of the behavior of 30 typhoons crossing the Philippines. In their analysis, the average translational speed of storms crossing the Philippines increased from about 5.5 m s^{-1} in the period before landfall, to over 6 m s^{-1} at landfall, decreasing steadily until it reached the western coast, with a secondary maximum noted about 6 h after leaving the island. Their results also indicate a northward perturbation in the storm tracks as the tropical cyclones passed through the islands. Results by Kintanar and Amadore (1974) showed that over 50% of the typhoons landfalling in this region of Luzon exhibited an increase of at least 2.5 m s^{-1} in speed of movement just before landfall, with a similar decrease in speed as the storms left the western coast.

When analysis was made of the supplemental experiment performed without the vortex included, it was found that southerlies existed over the island where the storm was deflected to the north, spreading to the regions over the ocean west and north of Luzon. The maximum southerly wind component northwest of Luzon was about 4 to 5 m s^{-1} at about the 5 km level.

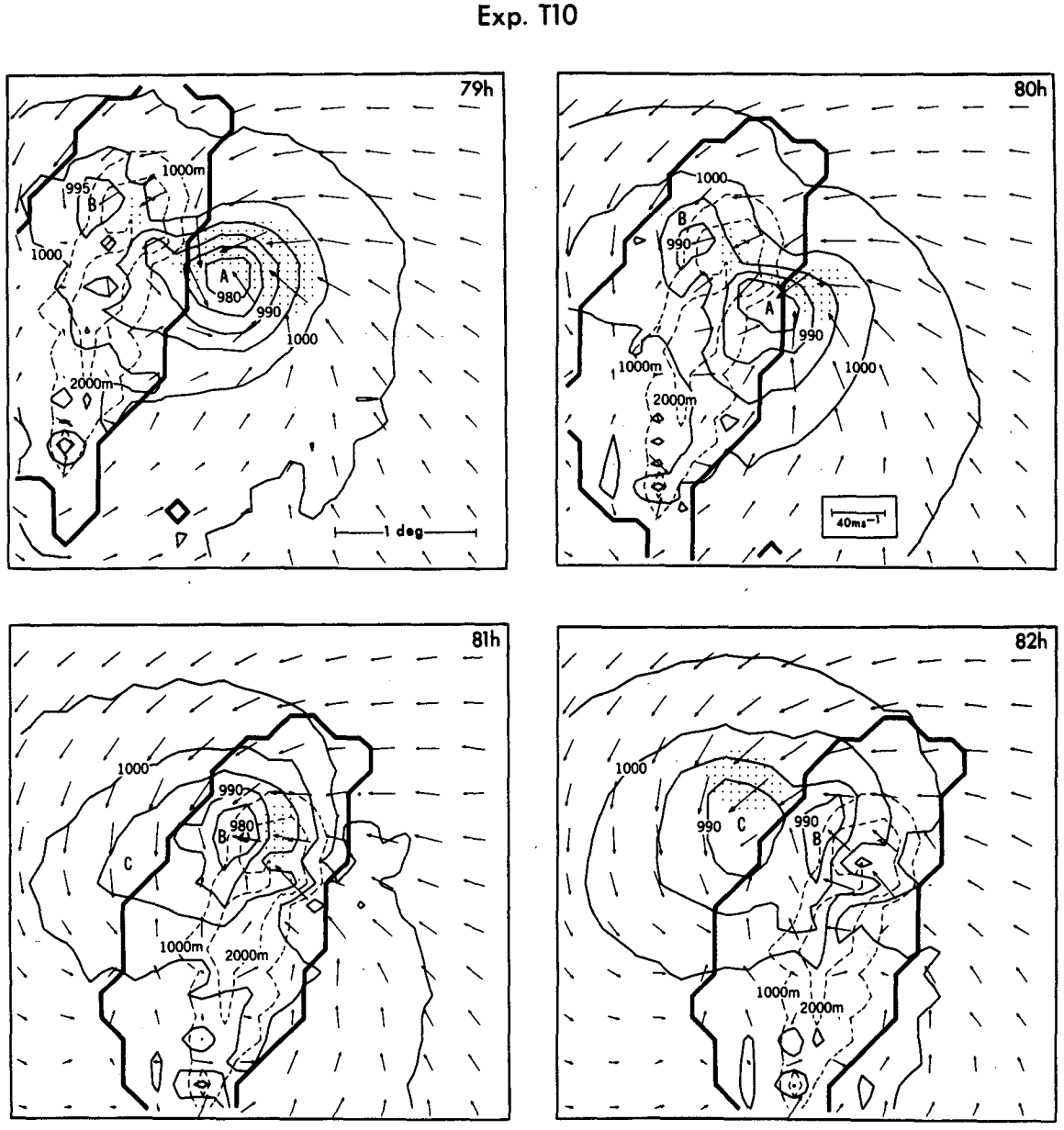

FIG. 15. Distribution of horizontal wind vectors plotted at every other point at model level 11 (σ = 0.992) in the finest mesh at 79, 80, 81 and 82 h, for Exp. T10. The sea level pressure is contoured, with the areas of hurricane force winds shaded. Systems A, B, and C, shown in Fig. 14, are indicated.

When the storm transversed this region during the period from 74 to 79 h, its average north–south translational speed was about 6.7 m s^{-1} compared to a value of 2.3 m s^{-1} during a 12 h time period when the storm was well east of Luzon. Southerlies of 5 m s^{-1} also occurred in some areas over the northern part of the island throughout much of the atmosphere. However, it is difficult to determine whether the changes in the storm's track and translational speed were caused primarily from this interaction of the basic flow with the topography or by the additional interaction of the storm with the island topography.

In a second supplemental experiment, run with the cool, flat, land surface condition, the storm showed a small northward deflection in its path compared to the ocean-only control, beginning about 5 h before landfall. It reached the coast about 20 km north of the ocean control. During the 10 h period that it transversed the island, the storm underwent significant weakening and the minimum sea level pressure rose 19 mb. When it

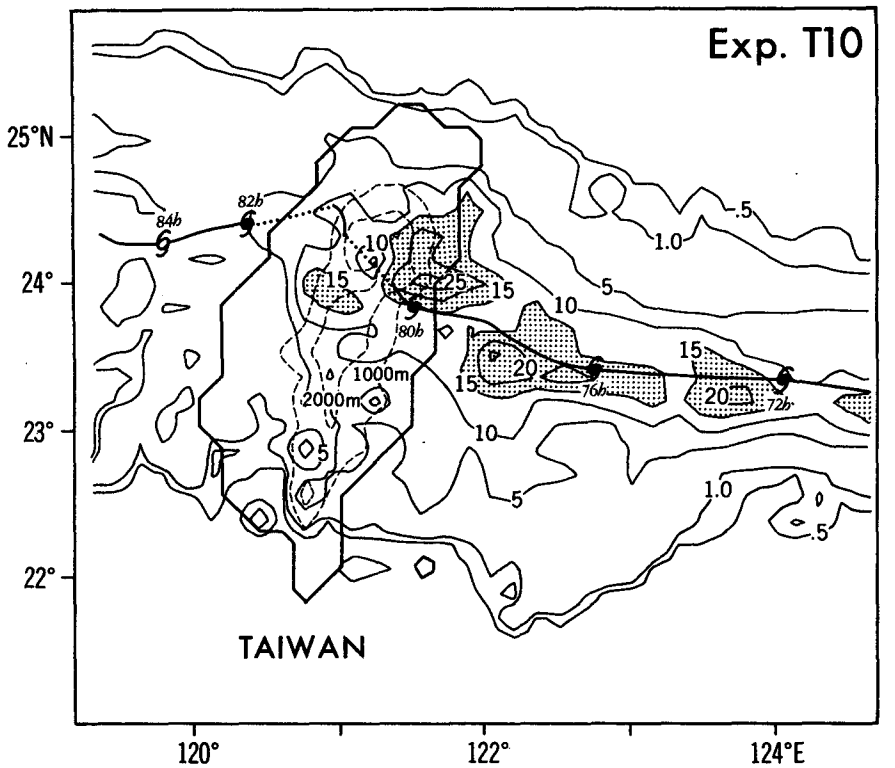

FIG. 16. Distribution of the storm total rainfall (cm) for Exp. T10. Total rainfall greater than 15 cm is shaded. The mountain heights are contoured at 1000 m intervals with the shoreline indicated with a thick solid line. The storm track of the minimum surface pressure is shown with the position of the storm center indicated at 4 h intervals unless otherwise indicated.

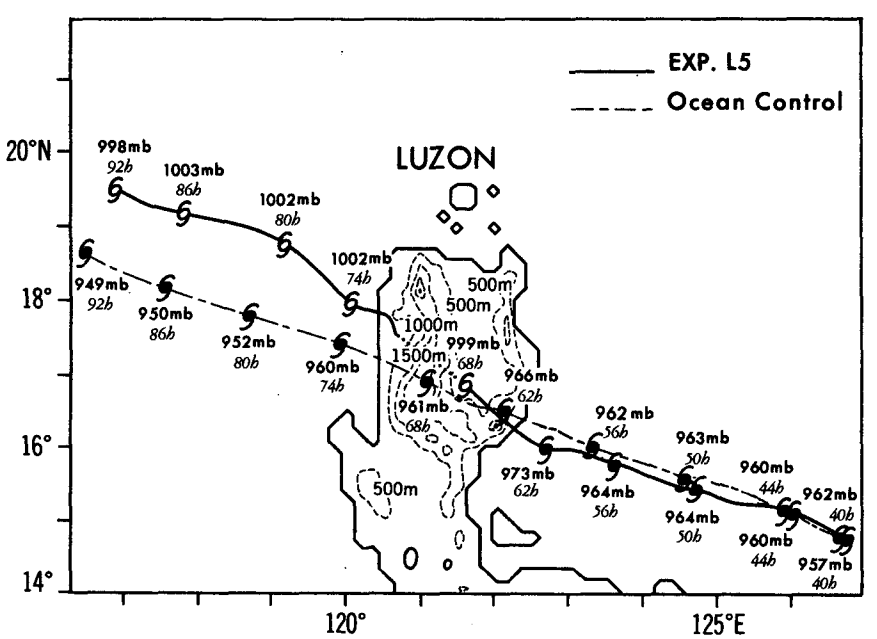

FIG. 17. Storm track for Exp. L5 (solid line) and the ocean-only control case (dashed line). The topographical distribution of Luzon used in Exp. L5 is shown. Storm positions are plotted every 6 h and indicated by a tropical cyclone symbol. (See Fig. 2 for more details.)

left the island it was located about 17 km north-northwest of the storm in the ocean control. In comparison, the storm in Exp. L5 was located about 68 km north of the ocean control when it reached Luzon's western coast.

The storm track for Exp. L10 is presented in Fig. 18. Similar to the previous simulation, the storm began to deviate to the left upstream of the island. By landfall, the storm was located about 30 km to the south of the position of the storm in the ocean control run. After landfall the surface low eventually tracked to the northwest, although it became hard to clearly identify over the mountainous terrain until it reformed on the western side of the mountain range, at a position about 50 km south of Exp. L5. After leaving Luzon the surface pressure center continued to move in a direction similar to the control case.

The storm tracks of three observed typhoons that passed through northern Luzon are presented in Fig. 19. Only Louise exhibited a distinct northward deflection as the storm passed through the island, although a small northward perturbation in the storm track of Typhoon Ivy can be seen about 8 h before it reached the island. In all three cases the storm's minimum sea level pressure began to fill upstream of the island. Upon leaving the island, Typhoons Georgia and Ivy began to reintensify when the storm centers were about 250 km west of the coast of Luzon. For Typhoon Louise the deepening of the storm's central pressure did not begin until the storm was about 350 km to the west of the island. These decay and redevelopment features are in good agreement with both Exps. L5 and L10 as discussed in subsection b.

b. Storm decay and redevelopment

Significant differences in the minimum sea level pressure between Exp. L5 and the ocean control run began about 8 h before landfall (see Fig. 17), again as drier air reached the storm circulation. Actually, slightly drier air (20 to 21 g kg^{-1}) reached the storm as early as 40 h of the simulation, as air from southern Luzon was advected north into the storm region. However, this drying appeared to have little effect in the storm's overall decay. The maximum low-level winds began to significantly decrease about 4 h before landfall, from a value of 47 to 40 m s^{-1} at landfall. When the storm left the western end of the island the maximum low level wind was about 25 m s^{-1}. Likewise, the minimum sea level pressure at landfall was 986 mb, with a 6 h filling rate of 26 mb centered at the landfall position. The observations of Brand and Blelloch (1973) also noted an average decrease in maximum surface winds from about 47 m s^{-1} beginning about 4 h before the typhoons reached the Philippines to approximately 45 m s^{-1} at landfall, finally decreasing to 31 m s^{-1} after the storms left the islands.

For Exp. L10, the storm's minimum sea level pressure did not undergo significant filling until about 1½ h before landfall. The minimum sea level pressure when the storm reached the coast was 978 mb. After landfall, as the storm began to ascend the eastern mountain range, very rapid decay occurred. For example, during the time between 45 and 46 h, the storm's minimum sea level pressure rose about 13 mb, to 992 mb. During this same time the storm's warm core rapidly weakened, with the average temperature difference at 8.1

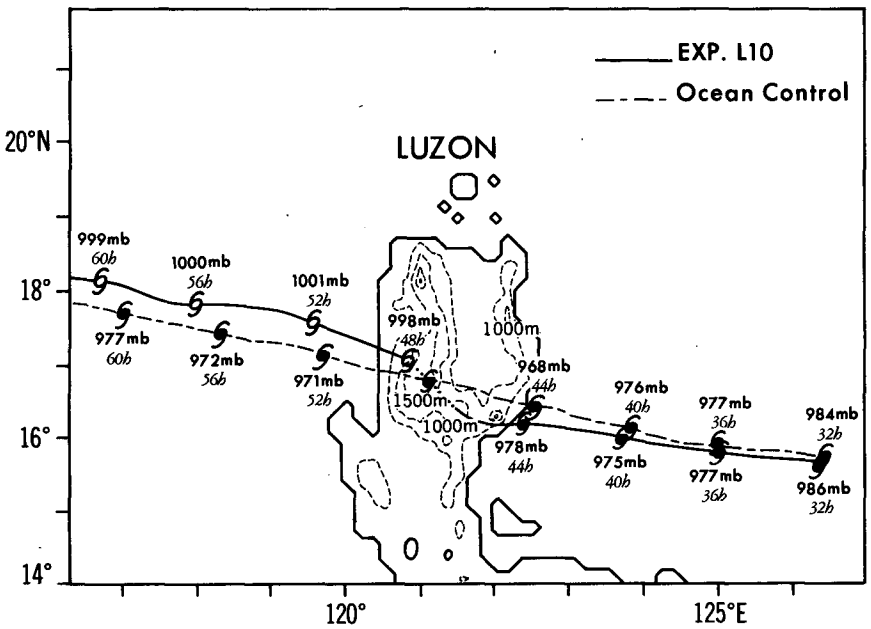

FIG. 18. As in Fig. 17 but for Exp. L10 and the 10 m s^{-1} ocean-only control case. Also, storm positions are plotted every 4 hours.

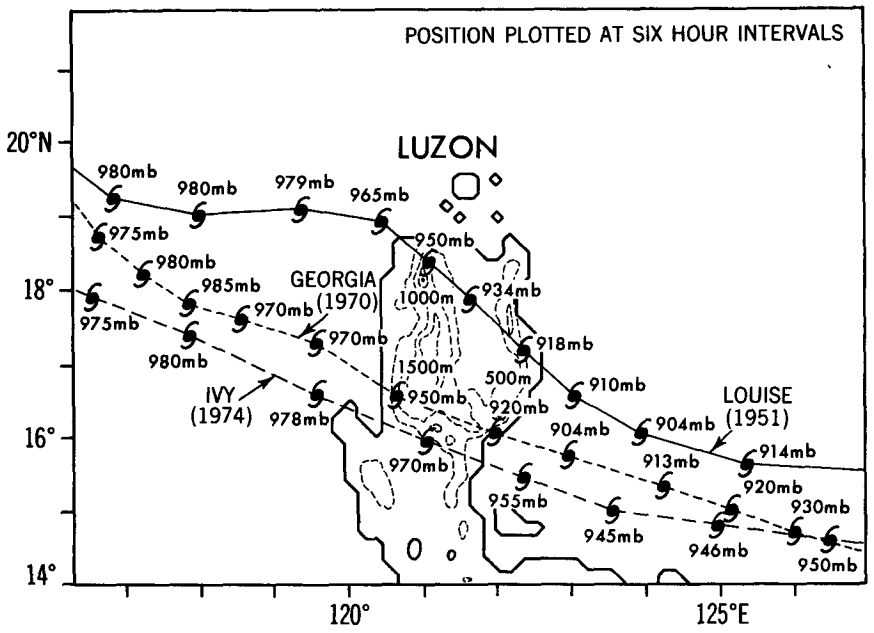

FIG. 19. Storm tracks for observed tropical cyclones that passed through northern Luzon, namely Louise, Georgia, and Ivy. The topographical distribution of Luzon that was used in the model simulations is shown. The storm positions were plotted at 6 h intervals, with the storm's minimum sea level pressure indicated. The storm tracks and data were obtained from the dataset compiled at the Shanghai Typhoon Institute (1984).

km height measured between the storm center and a 50 km radius decreasing about 40%.

In order to explain this rapid deterioration of the storm system, a heat budget was calculated for the moving storm at the 8.1 km height which is near the level of the maximum warm core. The equation for the change of temperature for the system moving with the storm can be written as

$$\frac{DT}{Dt} = \mathrm{TA} + \mathrm{TB} + \mathrm{TC} + \mathrm{TD} \qquad (5.1)$$

where

TA the change due to the relative horizontal advection $-(\mathbf{v} - \mathbf{c}) \cdot \nabla T$,
TB the change due to vertical motion $-\omega(\partial T/\partial p - \alpha/c_p)$,
TC the change due to condensation,
TD the change due to diffusion.

In the above equation, D/Dt denotes the change relative to the moving system, c is the mean storm movement vector, v the horizontal wind, ω the vertical velocity in pressure coordinates, ∇ the horizontal gradient operator, c_p the specific heat at constant pressure and α the specific volume. The budget was calculated at 45 h when the storm was located just south of a 1500 m mountain peak and very rapid decay was beginning. The values of the terms were compared to a budget calculated for a storm of similar intensity from the ocean control run (40 h). It was found that in the regions near the storm center, the maximum cooling rate due to the vertical motion, TB, increased from about -14.0×10^{-3} K s^{-1} for the ocean case to -15.7×10^{-3} K s^{-1} for the storm moving over Luzon. At the same time, as much drier air was being advected into the storm center from the mountain peaks over the island, the heating rate due to condensational heating, TC, decreased from 15.0×10^{-3} K s^{-1} for the ocean case to 13.9×10^{-3} K s^{-1} centered near the mountain peak. A large area of negative temperature tendency thus resulted in Exp. L10, and the intensity of the warm core weakened rapidly during the next hour. This significantly contributed to the deterioration of the entire storm system.

For both Exp. L5 and L10, as the storm system encountered the western mountain range barrier the surface low subsequently reformed on the western side. In both cases, the storm circulation center became vertically tilted with height. The lower (2 km) circulation center reformed to the south of the surface low, then drifted northwest. Figure 20 shows an example for Exp. L5. In this figure, the circulation center at 6.8 km was plotted, since the center became poorly defined west of the island at the higher levels until 85 h. Similar to the case of Taiwan, the path of the upper level circulation center was continuous as it crossed Luzon. Its center remained well south of the surface pressure center until about 92 h. From Fig. 20 we also can see that after the storm crossed the western coast, the upper-

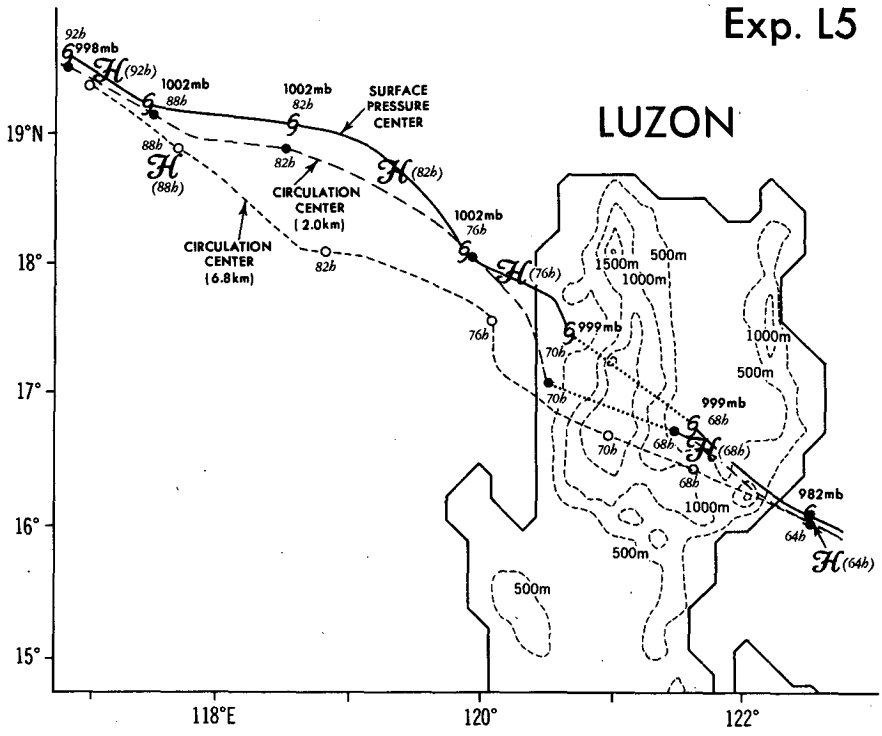

FIG. 20. Tracks and positions of the storm's sea level pressure (solid line and tropical cyclone symbol), and the center of circulation of the wind field at the 2 km (long dashed line and closed circle) and 6.8 km (short dashed line and open circle) heights for Exp. L5. Positions of the 8.1 km warm core (letter $\mathscr{H}$) are given. The coastline of northern Luzon is indicated by a thick solid line with the topographical heights contoured (thin dashed line). When the tracks were not continuous the positions were connected by a dotted line.

level warm core, which was associated with the area of maximum precipitation, was displaced by a considerable distance from the upper-level circulation center and the surface pressure center. It should be noted that although moist air was again advected into the storm region after the storm moved well west of Luzon, the storm did not undergo reintensification until 87 h, when the entire system tended to again become vertically coherent.

At 83 h the upper level warm core was located 90 km to the east of the surface pressure center. During the next hour this warm core region weakened while a new warm region developed to the south of the storm. At 85 h the warm core was about 50 km directly to the south of the surface pressure center (Fig. 21). This new warm core at the 8.1 km level underwent continual intensification from 84 h until the end of the integration at 92 h. The mean temperature difference between the warm core center and the region at a 150 km radius surrounding it increased from about 2 K at 84 h to 4.5 K by 89 h. To analyze quantitatively this intensification of the warm core, a heat budget (5.1) was computed at 84 h (Fig. 22). At this time only a small sign of the warm core observed at 83 h still remained. A strong cooling tendency in the advective term TA (-0.6×10^{-3} K s^{-1} maximum) was found at this location 1 h earlier (83 h), partly contributing to the strong cooling that was occurring there. By 84 h the net temperature tendency in this area was still generally negative, and the ventilation term (TA) was still importing cooler air into the region. However, a very large net positive tendency, with a maximum of over 1.9×10^{-3} K s^{-1}, was now located in the region of the new warm core as significant convection began to occur in this area. The value of the condensational heating term (TC) at this point was 3.6×10^{-3} K s^{-1} with a corresponding cooling tendency in the vertical motion term (TB) at the same point of -1.9×10^{-3} K s^{-1}. Since the ventilation term at this point was 0.26×10^{-3} K s^{-1} and the diffusion term was negligible compared to the other terms, the net result was a very large positive tendency and rapid strengthening of the warm core. As the warm core continued to intensify, its position became nearer to the upper-level circulation center in the next several hours as the latter slowly shifted toward the surface pressure center. The sequence of these events appeared concurrent with the beginning of the deepening of the storm center (87 h) about 14 h after the storm had moved across the western coast of Luzon. This agrees favorably with the statistical results of Brand and Blel-

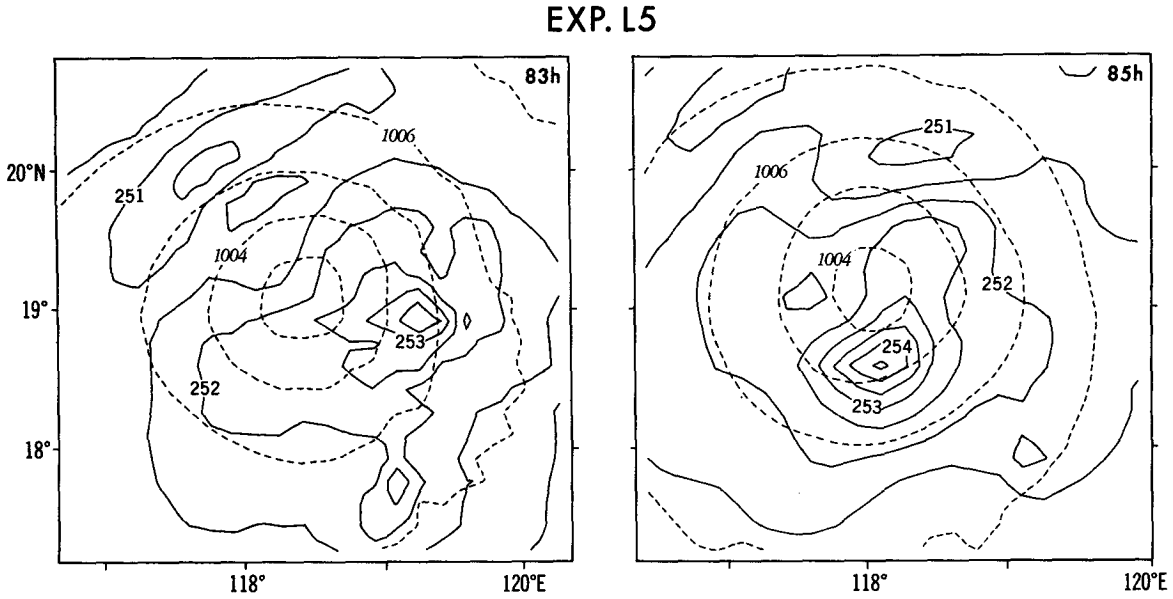

FIG. 21. Distribution for Exp. L5 of the sea level pressure field (mb, dashed line) and the temperature (K, solid line) at the 8.1 km height in the finest mesh at 83 and 85 h.

loch (1973), which showed that reintensification of storms typically begins about 12 h after they leave the western coast of the Philippines.

6. Comparison and summary of numerical results

The interaction of a tropical cyclone with different distributions of island topography has been analyzed for three separate regions: the islands of the Greater Antilles in the northern Caribbean, the northern Philippines (Luzon), and Taiwan. In this section the results will be compared with one another.

For all six cases in which the tropical cyclone approached islands with significantly high mountain ranges, the storm's translational speed increased before or upon landfall and the storm was deflected to the north. For the 5 m s^{-1} basic flow over Taiwan, the deflection to the north and acceleration in the translational speed began well upstream of the island. For the other cases most of the storm acceleration began just before landfall, and northward deflection of the path occurred over the mountainous terrain in good agreement with many observations and statistical studies. The storms were deflected to the left upwind of Hispaniola and Luzon compared to the positions of the ocean control. For the case of Luzon this deflection appeared to be similar to the upwind behavior of the tropical cyclone numerically simulated in Exp. M of BTK for a very long and wide mountain range.

The primary reason for the sharp deflection to the north over Hispaniola was the presence of southerlies that existed in this region throughout much of the atmosphere, generated by the interaction of the island topography with the basic flow. The mountain range of Taiwan caused the basic flow upwind of the island to curve to the north in the lower atmosphere for the 5 m s^{-1} case. As the storm approached the island, an additional interaction of the storm with the topography occurred, causing a significant acceleration of the translational speed, beginning about 6 h before landfall. For the 10 m s^{-1} easterly flow case, the basic flow was not significantly affected by the island topography, and the storm was deflected very little before landfall. This also was consistent with some observations. For Luzon, the basic flow over and west of the island curved to the north over much of the atmosphere. The storm was deflected to the north in these regions. This is similar to the northward deflection of the storm on the west side of the mountain range in Exp. M of BTK. Caution must be taken, however, in making comparisons with Exp. M since the limited north–south extent of the mountain ranges in these island experiments enabled flow to occur around the mountain ranges. Also, the much steeper vertical slope caused more significant blocking, especially in the case with the weaker basic flow (Pierrehumbert, 1984).

From Table 3 we see that the deflection of the storms was generally larger with the weaker easterly flow. For Hispaniola and Luzon, this possibly was due partly to the longer time period that the slower moving storms were influenced by the southerly flow found over the islands. The total northward displacements are comparable to the mean forecast error for the National Hurricane Center's Atlantic tropical cyclone track forecast. For example, during the period from 1970–79, the 12 and 24 h mean forecast error was 94 km

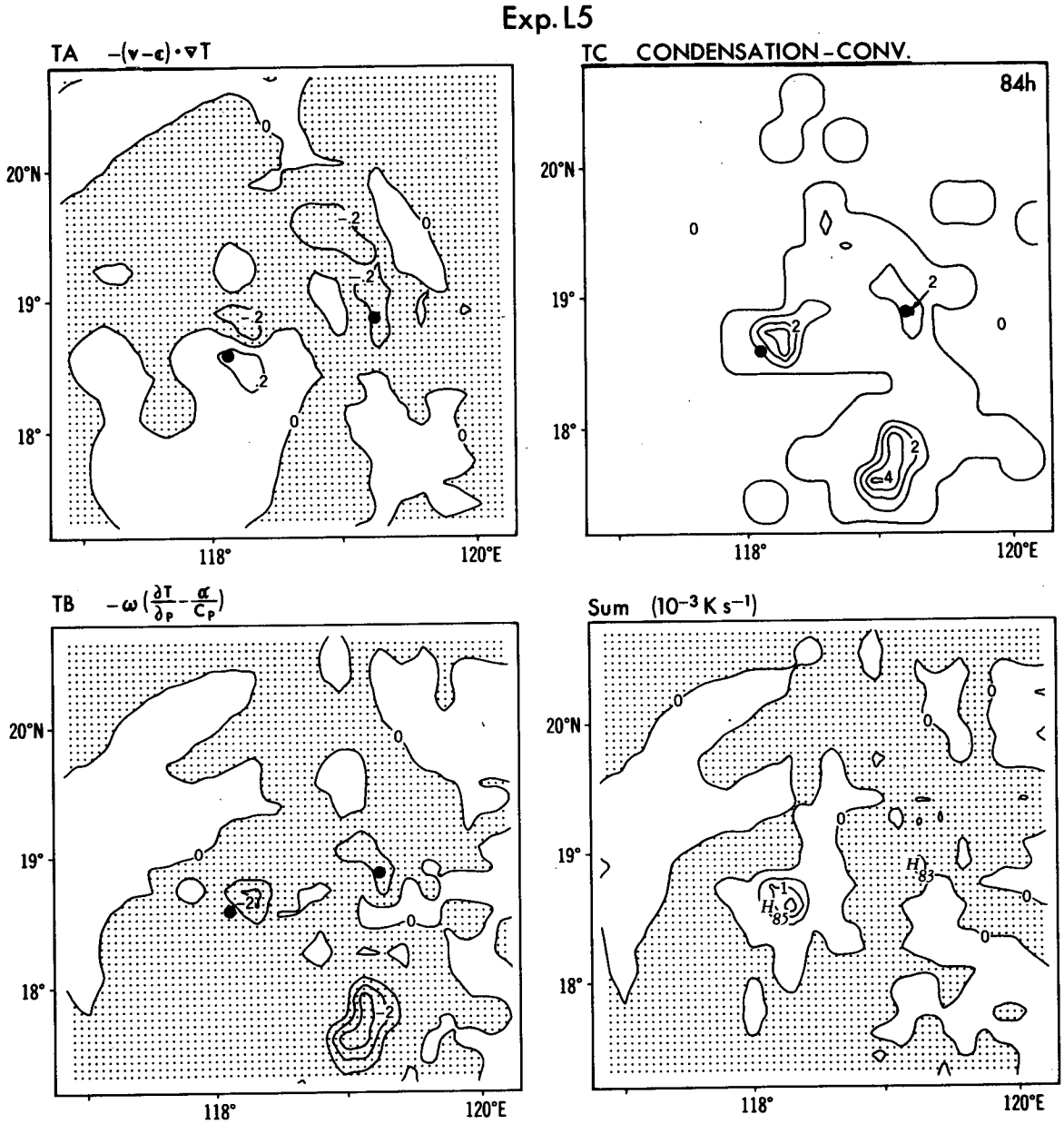

FIG. 22. Distribution for Exp. L5 of components and sum (10^{-3} K s^{-1}) of the heat budget equation (5.1) at the 8.1 km height in the finest mesh, computed relative to the moving storm at 84 h. Areas of negative values are shaded. The diffusion term (TD) was much smaller than the other terms and was not plotted. Positions of the old (H_{83}) and new (H_{85}) warm core are indicated at the bottom right figure, with their positions indicated by a closed circle in the other three figures.

and 202 km, respectively (Neumann and Pelissier, 1981). This indicates the importance that this effect may have in track forecasts in some cases.

All six of the storm cases showed decay upwind of the mountainous islands. The primary cause of the weakening was the influx of dry air into the storm circulation. The decay rate before landfall was less with the 10 m s^{-1} basic flow in all cases, as we see again in Table 3. All six cases showed considerable decay over the island mountain ranges. When the storms left the islands, the maximum low-level winds associated with the storm system were greater in the experiments with the stronger basic flow. After the storm landfall over Cuba, which is flat in comparison to the other island distributions, the storm's minimum central pressure weakened only about 4 mb (Exp. C5). This reduced weakening appeared to be due to the influx of moist air from the ocean area.

A large tilt in the storm's circulation center was found for both Exp. L5 and Exp. L10 as the storm

TABLE 3. Comparison of some of the key features of the six landfall simulations discussed.

	Movement		Decay				Rainfall	
Island experiment	Displacement at landfall relative to control Exp.; northward (+); southward (−) (km)	Difference in northward movement over islands between Exp. and control (km)	Maximum vertical tilt of circulation centers during integration (8.1 km–2 km) (km)	Upstream 12 h filling of minimum sea level pressure (mb)	Maximum low-level wind 12 h before landfall ($m\ s^{-1}$)	Maximum low-level wind leaving island ($m\ s^{-1}$)	Maximum total storm rainfall over island (cm)	Other special features of experiment
Hispaniola								
(Exp. C5)	−38	80	None	19	51	26	22.6	Southward deflection before landfall relative to control; northward deflection over island
(Exp. C10)	−18	48	None	9.2	47	31	18.4	Southward deflection before landfall relative to control; northward deflection over island
Taiwan								
(Exp. T5)	112	20	40	33	48	27	22.5	Accelerated movement to the northwest well east of Taiwan
(Exp. T10)	5	40	50	8.7	48	42	27.6	Formation of secondary lows
Luzon								
(Exp. L5)	−20	90	120	22.1	48	25	25.1	Northwest movement over islands; reintensification well west of Luzon.
(Exp. L10)	−30	67	100	6.7	40	30	19.6	Northwest movement over islands; very rapid decay just after landfall; reintensification well west of Luzon.

system was leaving the western coast of Luzon. A smaller tilt was found in Exp. T10 as the storm passed over the island of Taiwan. In contrast, however, for expt T5 the tilting of the circulation centers began when the storm was still upstream of the island. This effect probably resulted from the directional wind shear that existed in this region east of Taiwan. For the island of Hispaniola, no tilting of the circulation centers was found at any time, as the storm crossed the island.

Reintensification of the storm system began immediately after the storm passed over Hispaniola and again moved over open water. In contrast, although very moist air was eventually advected into the storm system, the storm did not reintensify after leaving the coast of Luzon until the upper and lower circulation centers and the surface pressure center all became vertically coupled again about ½ day later. For the case of Taiwan the storm continued to weaken after passing west of Taiwan as much drier air was still being advected into the storm system by the end of the experiment.

7. Conclusion

The behavior of tropical cyclones in the presence of mountainous island distributions was numerically simulated using a triply nested, movable mesh model. Although the experiments were all performed for an idealized flow and experimental design, many of the results obtained agreed well with statistical and observed studies regarding important storm features such as change in translational speed, deflection of the storm path, storm decay, reintensification, and development of secondary surface lows. The simplified experimental design has enabled these effects of the island terrain to be isolated and easily analyzed. Although we cannot generalize the obtained numerical results for all observed cases, especially those involving more complicated flow fields, this research has led to improved understanding and explanation of some of the behavior of tropical cyclones in regions of mountainous islands.

The following are what we confirmed or can speculate from the present numerical study:

- The island topography affects the basic flow field, in some cases well upstream of the islands. It also directly influences the structure of the tropical cyclones when they pass over or nearby the region. Combination of the above two effects yields changes in the movement and structure of the tropical cyclones.
- For the cases considered, the storm tracks show northward deflection, sometimes after a small southward deflection. The northward deflection is generally larger and sometimes begins further upstream in the case of the weaker zonal flow. The translational speed of the storms also tends to increase along with the deflection.
- After making landfall and encountering the high mountain ranges, the surface pressure minimum undergoes rapid filling. The surface low may continue to move along with the upper-level vortex as it crosses the mountain range (e.g., the Hispaniola case in this study), or may become obscure before reforming on the lee side slope (e.g., Luzon cases). Sometimes (e.g., one of the Taiwan cases) a secondary surface low or lows form behind the mountain range. In this case, it appears that the upper-level vortex becomes detached from the original surface low and eventually couples with the secondary one.
- The latent energy supply as well as the vertical coherence of the storm system are important factors in the determination of the intensity change of the storms near and over the islands. When dry air is advected from the mountain region into the storm area, the storm may exhibit a weakening tendency even well before landfall. The weakening may be enhanced if the vertical axis of the storm system is forced to tilt at the same time. After leaving the island and moving over open ocean, the storms generally reintensify if a vertically coherent structure is present, or, otherwise, not until it is reestablished several hours later.

As mentioned, the storm structure often became disorganized over and after crossing the island terrain, with the location of the warm core or area of intense precipitation, upper and lower circulation centers and the surface pressure center displaced from one another. This implies that care must be taken to determine the storm position from surface, upper air or satellite observations. For example, for the case of the experiment for Luzon, we found that the area of heavy rainfall at one time period was displaced over 120 km from the surface pressure and circulation center.

Finally, we have shown that in the cases involving significant mountain heights, detailed topography should not be neglected in numerical models if accurate forecasts of the storm track and behavior are to be made. This point is suggestive for improvement of storm prediction, since high mountain ranges are found in many of the areas with significant tropical cyclone activity.

Acknowledgments. The authors would like to thank J. Mahlman for his continuous support of the hurricane dynamics project at GFDL. They are grateful to S. Chang of the Naval Research Laboratory and Y.-H. Pan of the Institute of Atmospheric Physics, Academia Sinica, for supplying us with some of the observed storm tracks and information used throughout the text. They would also like to express their appreciation to L. Shapiro of the Hurricane Research Division of AOML, and S. Brand of the Naval Environmental Prediction Research Facility for their valuable comments and criticisms on the original version of this manuscript. Thanks is also given to an anonymous reviewer who supplied useful information on the tracks of tropical cyclones in the regions of the western Atlantic. Special thanks and credit is also given to P. Tunison, K. Raphael, J. Varanyak, M. Zadworny and

J. Conner for preparing the figures, and to J. Kennedy for typing part of the manuscript.

REFERENCES

Bender, M. A., R. E. Tuleya and Y. Kurihara, 1985: A numerical study of the effect of a mountain range on a landfalling tropical cyclone. *Mon. Wea. Rev.*, **113,** 567–582.

Brand, S., and J. W. Blelloch, 1973: Changes in the characteristics of typhoons crossing the Philippines. *J. Appl. Meteor.*, **12,** 104–109.

——, and ——, 1974: Changes in the characteristics of typhoons crossing the island of Taiwan. *Mon. Wea. Rev.*, **102,** 708–713.

——, J. C. Herb, J. C. Woo, J. J. Lou and M. Danard, 1982: Mesoscale effects of topography on tropical cyclone-associated surface winds. *Papers in Meteorological Research,* (Taiwan), **5,** 37–49.

Brunt, A. T., 1968: Space–time relations of cyclone rainfall in the northeast Australian region. *Civil Eng. Trans. Inst. Eng. Australia,* April issue, 40–46. Inst. of Eng. Australia, 11 National Circuit, Barton A.C.T. 2600, Australia.

Chang, S. W., 1982: The orographic effects induced by an island mountain range on propagating tropical cyclones. *Mon. Wea. Rev.*, **110,** 1255–1270.

Hamuro, M., Y. Kawata, S. Matsuda, T. Matsuno, N. Nakamura, F. Pak, T. Takeda and M. Yanai, 1969: Precipitation bands of Typhoon Vera in 1959 (Part I). *J. Meteor. Soc. Japan,* **47,** 298–308.

Hebert, P. J., 1980: Atlantic hurricane season of 1979. *Mon. Wea. Rev.*, **108,** 973–990.

Kasahara, A., 1966: The dynamical influence of orography on the large-scale motion of the atmosphere. *J. Atmos. Sci.*, **23,** 259–271.

Kintanar, R. L., and L. A. Amadore, 1974: Typhoon Climatology in Relation to Weather Modification Activities. WMO-No. 408. World Meteorological Organization, Secretariat: CP 5, CH-1211, Geneva 20, Switzerland.

Kurihara, Y., 1973: A scheme of moist convective adjustment. *Mon. Wea. Rev.*, **101,** 547–553.

——, and M. A. Bender, 1980: Use of a movable nested mesh model for tracking a small vortex. *Mon. Wea. Rev.*, **108,** 1792–1809.

Manabe, S., and J. L. Holloway, 1975: The seasonal variation of the hydrologic cycle as simulated by a global model of the atmosphere. *J. Geophys. Res.*, **80,** 1617–1649.

Mellor, G. L., and T. Y. Yamada, 1974: A hierarchy of turbulence closure models for planetary boundary layers. *J. Atmos. Sci.*, **31,** 571–583.

Moss, M. S., and R. W. Jones, 1978: A numerical simulation of hurricane landfall. NOAA Tech. Memo. ERL NHEML-3, NOAA/AOML/HRD, 1–15. NTIS PB-290398/7GA.

Neumann, C. J., and J. M. Pelissier, 1981: An analysis of Atlantic tropical cyclone forecast errors, 1970–1979. *Mon. Wea. Rev.*, **109,** 1248–1266.

Pao, H. P., and R. R. Hwang, 1977: Effects of mountains on a typhoon vortex: A laboratory study. *Extended Abstracts for the 11th Technical Conf. on Hurricanes and Tropical Meteorology,* Miami Beach, 88–91. [Available from Amer. Meteor. Soc., 45 Beacon St., Boston, MA 02108]

Pierrehumbert, R. T., 1984: Linear results on the barrier effects of mesoscale mountains. *J. Atmos. Sci.*, **41,** 1356–1367.

Shanghai Typhoon Institute, 1984: Basic data of western north Pacific typhoons, 1949–1980 (in Chinese). Meteorology Press, Beijing.

Smith, R. B., 1979: The influence of mountains on the atmosphere. *Ad. Geophys.*, **21,** 87–230. Academic Press.

Sugg, A. L., 1967; The hurricane season of 1966. *Mon. Wea. Rev.*, **95,** 131–142.

Tuleya, R. E., and Y. Kurihara, 1978: A numerical simulation of the landfall of tropical cyclones. *J. Atmos. Sci.*, **35,** 242–257.

——, M. A. Bender and Y. Kurihara, 1984: A simulation study of the landfall of tropical cyclones using a movable nested-grid model. *Mon. Wea. Rev.*, **112,** 124–136.

Wang, S. T., 1980: Prediction of the behavior and strength of typhoons in Taiwan and its vicinity (in Chinese). Res. Rep. 018, Chinese National Science Council, Taipei, Taiwan. [Available from the author at Central Weather Bureau, 64 Kung-Yuan Road, Taipei, Taiwan.]